THE EMBO JOURNAL

Splicing factor YBX1 regulates bone marrow stromal cell fate during aging

Ye Xiao[1,†] , Guang-Ping Cai[1,†], Xu Feng[1], Yu-Jue Li[1], Wan-Hui Guo[1], Qi Guo[1], Yan Huang[1], Tian Su[1], Chang-Jun Li[1], Xiang-Hang Luo[1,2], Yong-Jun Zheng[3,*] & Mi Yang[1,2,**]

Abstract

Senescence and altered differentiation potential of bone marrow stromal cells (BMSCs) lead to age-related bone loss. As an important posttranscriptional regulatory pathway, alternative splicing (AS) regulates the diversity of gene expression and has been linked to induction of cellular senescence. However, the role of splicing factors in BMSCs during aging remains poorly defined. Herein, we found that the expression of the splicing factor Y-box binding protein 1 (YBX1) in BMSCs decreased with aging in mice and humans. YBX1 deficiency resulted in mis-splicing in genes linked to BMSC osteogenic differentiation and senescence, such as *Fn1*, *Nrp2*, *Sirt2*, *Sp7*, and *Spp1*, thus contributing to BMSC senescence and differentiation shift during aging. Deletion of *Ybx1* in BMSCs accelerated bone loss in mice, while its overexpression stimulated bone formation. Finally, we identified a small compound, sciadopitysin, which attenuated the degradation of YBX1 and bone loss in old mice. Our study demonstrated that YBX1 governs cell fate of BMSCs via fine control of RNA splicing and provides a potential therapeutic target for age-related osteoporosis.

Introduction

Bone marrow stromal cells (BMSCs) are heterogeneous and primitive cells resident in the bone marrow, which have the ability to differentiate into a variety of cell types, including osteoblasts, adipocytes, and chondrocytes (Pittenger *et al*, 1999; Sekiya *et al*, 2004; Guilak *et al*, 2009). BMSCs directly contribute to bone remodeling by differentiating into osteoblasts. The increasing rate of senescence of BMSCs and their enhanced tendency to differentiate into adipocytes rather than osteoblasts during aging lead to bone marrow fat accumulation and bone loss, eventually resulting in osteoporosis and fragility-related fractures (Li *et al*, 2015, 2017, 2018; Chen *et al*, 2016). However, the molecular mechanism of senescence and age-associated lineage shift of BMSCs remains elusive.

Previous research on the molecular mechanism of senescence and age-associated lineage shift in BMSCs has mostly focused on transcriptional regulation. However, recent findings revealed the underrated role of alternative splicing (AS) in BMSC senescence and differentiation (Park *et al*, 2020). Alternative splicing of precursor mRNA (pre-mRNA) is an important posttranscriptional regulatory pathway of more than 90% of multiexon protein-coding genes in mammals, enabling cells to generate abundant transcripts and protein diversity from a limited number of genes (Lee & Rio, 2015). Most human genes undergo AS (Pan *et al*, 2008) in a variety of physiological and pathological processes, such as mesenchymal stem cell differentiation, tissue and organ development, aging, and tumorigenesis (Baralle & Giudice, 2017; Urbanski *et al*, 2018; Bowler & Oltean, 2019; Bhadra *et al*, 2020; Park *et al*, 2020). In BMSCs, the expression of genes related to senescence such as *P53* (encoding tumor protein P53)/*P16* (encoding cyclin dependent kinase inhibitor 2A), or key transcription factors related to differentiation such as *RUNX2* (encoding RUNX family transcription factor 2) or *PPARG* (encoding peroxisome proliferator activated receptor gamma) could be regulated by AS (Milona *et al*, 2003; Makita *et al*, 2008; Deschenes & Chabot, 2017; Aprile *et al*, 2018).

Dysregulation of pre-mRNA splicing is associated with aging, and a large proportion of age-related changes in AS are associated with alternations of the expression of splicing factors (Southworth *et al*, 2009; Harries *et al*, 2011; Mazin *et al*, 2013). However, whether the changes in the activity of splicing factors and in the production of key splice variants in BMSC genes would impact cellular senescence and fate determination of BMSCs during aging is unknown. Y-box binding protein 1 (YBX1) is a multifunctional protein known to participate in a wide variety of DNA/RNA-dependent events, including DNA reparation and transcription, pre-mRNA splicing, mRNA stability, and translation (Kohno *et al*, 2003; Skabkin *et al*, 2006; Eliseeva *et al*, 2011). YBX1 has been reported to control the expression of pluripotency-related genes in embryonic stem cells (Guo *et al*, 2016). YBX1 could

1 Department of Endocrinology, Endocrinology Research Center, Xiangya Hospital of Central South University, Changsha, China
2 National Clinical Research Center for Geriatric Disorders, Xiangya Hospital, Changsha, China
3 Department of Burn Surgery, The First Affiliated Hospital of Naval Medical University, Shanghai, China
   *Corresponding author. Tel: +86 021 31161826; Fax: +86 021 31161828; E-mail: smmuzhengyongjun@163.com
   **Corresponding author. Tel: +86 0731 89752728; Fax: +86 0731 84327332; E-mail: ym2405@csu.edu.cn
   †These authors contributed equally to this work

also regulate multiple biological activities, including cell proliferation, differentiation, senescence, apoptosis, and tumor development (Kotake *et al*, 2013; Lyabin *et al*, 2014; Evans *et al*, 2020; Xiao *et al*, 2020). It has been reported that YBX1 restrained cellular senescence by directly binding to the *P16* promoter and repressing the transcription of *P16* (Kotake *et al*, 2013). In past decades, as a splicing factor, the role of YBX1 in AS has been studied (Allemand *et al*, 2007; Dutertre *et al*, 2010; Wei *et al*, 2012; Marchesini *et al*, 2017; Jayavelu *et al*, 2020). Jayavelu *et al* (2020) reported that YBX1-mediated pre-mRNA splicing is the key mechanism of persistence of Janus kinase 2 (JAK2)-mutated myeloproliferative neoplasms. Ma *et al* (2020) demonstrated that YBX1 expression decreased with aging in six tissues (bone marrow, brown adipose tissue, white adipose tissue, aorta, skin, and liver) and participated in adipose stem cell maintenance in white adipose tissue. However, whether YBX1 regulates the fate of BMSCs via AS is unclear.

In this study, we observed altered pre-mRNA splicing and changed gene expression pattern in BMSCs during aging and further found that the expression of splicing factor YBX1 in BMSCs decreased with aging in mice and humans. YBX1 could stimulate osteogenic differentiation and restrain the senescence of BMSCs by regulating a cluster of genes, including *Fn1* (encoding fibronectin 1), *Nrp2* (encoding neuropilin 2), *Sirt2* (encoding sirtuin 2), *Sp7* (encoding Sp7 transcription factor, also known as osterix [OSX]), and *Spp1* (encoding secreted phosphoprotein 1) by acting as a splicing factor. Moreover, we discovered a natural small compound, sciadopitysin, which can restrain the degradation of YBX1 and attenuate age-related bone loss. Our results demonstrated that splicing factor YBX1 regulates the differentiation and senescence of BMSCs via fine control of RNA splicing, suggesting YBX1 as a potential therapeutic target for age-related osteoporosis.

Results

Dysregulated pre-mRNA alternative splicing and altered gene expression patterns in BMSCs during aging

Aging-related decline in bone formation is closely associated with the debility of BMSCs. BMSCs isolated from 24-month-old mice showed significant higher levels of senescence, indicated by β-Galactosidase (β-Gal) staining and lower osteogenic differentiation potential, as indicated by Alizarin Red staining, after osteogenic induction compared with BMSCs isolated from 2-month-old mice (Fig 1A–C; Appendix Fig S1A). Dysregulation of pre-mRNA splicing directly contributes to cell dysfunction and senescence (Baralle & Giudice, 2017; Deschenes & Chabot, 2017; Park *et al*, 2020). To investigate the splicing events and gene expression pattern in BMSCs during aging, we performed full-length transcriptome sequencing and AS analysis in BMSCs isolated from 2- and 24-month-old mice (Fig 1D). We evaluated changes in pre-mRNA splicing by calculating "percentage spliced in" (ΔPSI) values of several major alternative splicing events with ΔPSI > 0.1 and *P*-value < 0.05 (Fig 1E). Gene Ontology (GO) analysis showed that those changed AS-involved genes were related to osteoblast differentiation and cellular senescence (Fig 1E). Meanwhile, the BMSCs isolated from 24-month-old mice exhibited increased expression of a cluster of senescence and adipogenic differentiation-related isoform genes and decreased expression of a cluster of osteogenic differentiation-related isoform genes with at least a 1.3-fold change when compared with BMSCs isolated from 2-month-old mice (Fig 1F). Pre-mRNA splicing in BMSCs upon aging showed changes in alternative first exon events (35.98%), alternative 5′ splice sites (15.09%), exon skipping (14.76%), intron retention (13.93%), alternative last exons (11.44%), and alternative 3′ splice sites (8.46%) (Fig 1G). To investigate the potential splicing factor responsible for the AS events in BMSCs during aging, we identified 92 RNA splicing proteins whose expression level changed by at least 1.3-fold between BMSCs isolated from 2- and 24-month-old mice, by combining analysis of RNA sequencing data with RNA binding proteins and splicing factor datasets (Fig 1H). These differentially expressed splicing factors form a regulatory network whose functions are mainly enriched in terms related to various RNA metabolic processes (Fig 1I). We further screened out 50 differentially expressed proteins with functions enriched in mRNA splicing or regulation of RNA splicing (Fig 1I and J). The changed splicing factors and pre-mRNA altered splicing events might play an important role in the functional debility of BMSCs during aging.

Figure 1. Dysregulated pre-mRNA alternative splicing and altered gene expression patterns in BMSCs during aging.

A   Schematic diagram of the isolation and culture of BMSCs from 2- and 24-month-old mice. BMSCs, bone marrow stromal cells.

B   Representative images of β-Gal staining (left panel) and quantification of β-Gal-positive cells (right panel) of BMSCs isolated from 2- and 24-month-old mice. Scale bar: 100 μm. β-Gal, beta-galactosidase.

C   Representative images of Alizarin Red staining at 21 days of osteogenic induction (left panel) and quantification of calcification (right panel) of BMSCs isolated from 2-month-old and 24-month-old mice by detecting the amount of Alizarin Red extracted from the matrix.

D   Schematic diagram of the experimental process of alternative splicing analysis.

E   Gene ontology analysis of differentially expressed genes between BMSCs isolated from 2- and 24-month-old mice. ΔPSI, percentage spliced in.

F   Heat map of differentially expressed genes between BMSCs isolated from 2- and 24-month-old mice.

G   Histogram of the differential splicing events between BMSCs isolated from 2- and 24-month-old mice. AS, alternative splicing.

H   Venn diagrams of overlapping genes between differentially expressed genes, RNA-binding proteins, and splicing factor datasets between BMSCs isolated from 2- and 24-month-old mice.

I   Enrichment network representing the top 10 enriched terms of differentially expressed RNA splicing factors between BMSCs isolated from 2- and 24-month-old mice. Enriched terms with high similarity were clustered and rendered as a network, while each node represents an enriched term and is colored according to its cluster. The node size indicates the number of enriched genes, and the line thickness indicates the similarity score shared by two enriched terms.

J   The list of differentially expressed RNA splicing factors between BMSCs isolated from 2- and 24-month-old mice whose functions are clustered in mRNA splicing and regulation of RNA splicing.

Data information: In (B) and (C), *n* = 5 in each group from three independent experiments. In (E) and (F), *n* = 3 in each group. Data are shown as the mean ± SEM.
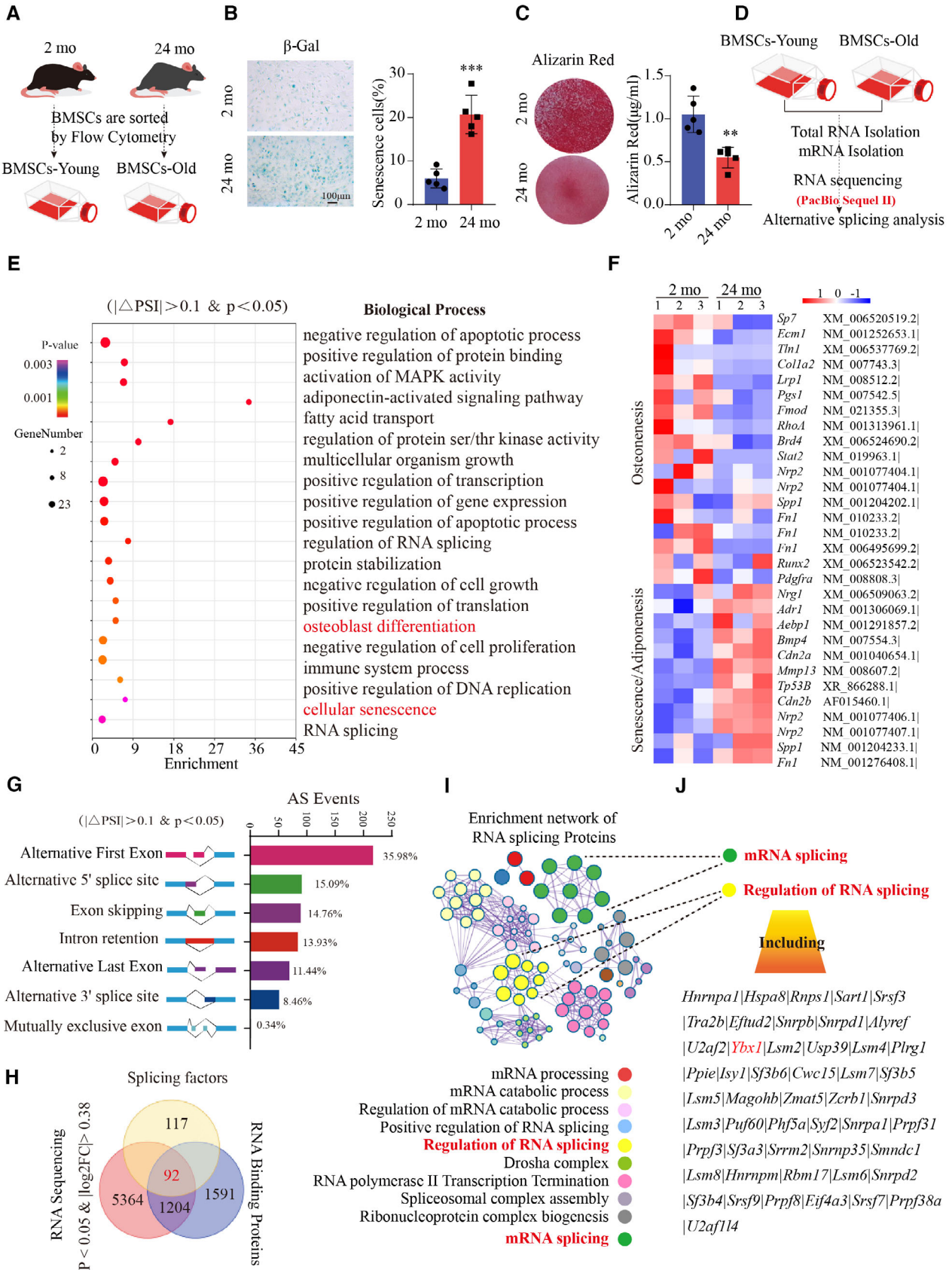**P < 0.01; ***P < 0.001; Student's *t*-test.

Figure 1.

Splicing factor YBX1 regulated the fate decision and senescence of BMSCs and showed decreased expression during aging

Among these changed RNA splicing factors was YBX1, inactivation of which has been reported to induce apoptosis in mouse and primary human cells and cause regression of malignant clones *in vivo* (Jayavelu *et al*, 2020). We confirmed the lower expression level of YBX1 in BMSCs isolated from 24-month-old mice relative to 2-month-old mice using immunofluorescence staining (Fig 2A and B), Western blotting (Appendix Fig S1B and C), and qRT-PCR (Appendix Fig S1D) analyses. The YBX1 level was also lower in cultured primary BMSCs from late passages (Appendix Fig S1E–H). Leptin receptor (LEPR)-positive cells in bone marrow represent a subset of mesenchymal stem cells (Zhou *et al*, 2014). Co-immunofluorescence staining of LEPR and YBX1 on the bone marrow confirmed the lower number of YBX1$^+$LEPR$^+$ cells in the metaphysis area in femurs of 24-month-old mice (Fig 2C and D). Similarly, the YBX1 level in human BMSCs also correlated negatively with age (Fig 2E). These results indicated that splicing factor YBX1 might play roles in the AS events in BMSCs during aging.

Reduced osteogenic differentiation tendency and enhanced adipogenic differentiation tendency are the characteristics of aging BMSCs. We found that the RNA and protein levels of YBX1 were upregulated during osteogenic induction and downregulated during adipogenic induction (Appendix Fig S1I–N). To further investigate the role of YBX1 in BMSC differentiation and senescence, we used adenovirus-mediated short hairpin RNA (shRNA) to knock down *Ybx1* in BMSCs and verified the knockdown efficiency using Western blotting (Appendix Fig S1O and P). BMSCs with depletion of YBX1 showed lower osteogenic capacity after osteogenic induction, as indicated by Alizarin Red staining (Fig 2F and G; Appendix Fig S1Q) and higher adipogenic differentiation ability after adipogenic induction, as indicated by Oil Red O staining (Fig 2H and I; Appendix Fig S1R). In addition, BMSCs with depletion of YBX1 had a higher percentage of β-Gal-positive senescent cells compared with the control group (Fig 2J and K). We confirmed the decreased expression of osteogenesis-related genes, and increased expression of adipogenesis and senescence-related genes using qRT-PCR in BMSCs with depletion of YBX1 (Fig 2L and M). RNA-Seq analysis also showed that osteogenic differentiation-related genes were downregulated but adipogenic differentiation and senescence-related genes were upregulated in BMSCs with depletion of YBX1 in comparison with the control group (Fig 2N).

Taken together, these results suggested that YBX1 plays a role in the regulation of BMSC senescence and fate decision.

Depletion of YBX1 in BMSCs resulted in accelerated bone loss and bone marrow fat accumulation

To further investigate the role of YBX1 on the fate decision and senescence of BMSCs *in vivo*, we crossed *Prx1* (peroxiredoxin 1)-*Cre* transgenic mice with *Ybx1$^{flox/flox}$* mice to specifically knock out *Ybx1* in BMSCs (*Ybx1$^{Prx1-CKO}$*). We confirmed the knockout efficiency in BMSCs using qRT-PCR analysis (Fig 3A).

Microcomputed tomography (μCT) analysis of the distal femur metaphysis revealed that the bone volume was significantly lower in *Ybx1$^{Prx1-CKO}$* male mice relative to their *Ybx1$^{flox/flox}$* littermates at 3 and 12 months old (Fig 3B and C). Additionally, depletion of YBX1 in BMSCs reduced the trabecular thickness and number, while increasing the trabecular separation (Fig 3D–F). Histochemistry and immunohistochemical analysis showed that *Ybx1$^{Prx1-CKO}$* mice had a significantly higher number of adipocytes in their bone marrow (Fig 3G and H), but lower number of osteoblasts on the trabecular bone surfaces (Fig 3I and J). The number of osteoclasts on the bone surface was unchanged in *Ybx1$^{Prx1-CKO}$* mice (Fig 3K and L). Calcein double labeling revealed that *Ybx1$^{Prx1-CKO}$* mice had a significantly lower trabecular bone mineral apposition rate (MAR) and bone formation rate (BFR) compared with those of their *Ybx1$^{flox/flox}$* littermates (Fig 3M–O). Consistently, the bone volume, and the trabecular thickness and number were also significantly lower, while the trabecular separation was significantly higher, in *Ybx1$^{Prx1-CKO}$* female mice relative to their *Ybx1$^{flox/flox}$* littermates at 3 months old (Appendix Fig S2A–E).

Leptin receptor (LEPR)-positive cells in bone marrow represent a subset of mesenchymal stem cells (Zhou *et al*, 2014). To further confirm the effect of BMSC YBX1 deficiency on bone formation, we also crossed *Lepr-Cre* transgenic mice with *Ybx1$^{flox/flox}$* mice to specifically knock out YBX1 in BMSCs (*Ybx1$^{lepr-CKO}$*), and confirmed the knockout efficiency using qRT-PCR analysis (Appendix Fig S3A). Consistently, *Ybx1$^{lepr-CKO}$* mice showed a significantly lower bone volume, trabecular thickness, trabecular number, and higher

Figure 2. Splicing factor YBX1 regulated fate decision and senescence of BMSCs and showed decreased expression during aging.

A, B Representative images (A) of immunofluorescence staining and quantification (B) of YBX1 (green) in primary BMSCs.

C, D Representative immunohistochemical staining images of YBX1 (red) and LEPR (green) (C) and quantification of YBX1$^+$ LEPR$^+$ cell numbers (D) in femoral bone marrow. MP, metaphysis; T Ar, Tissue area. Arrows point to YBX1$^+$ LEPR$^+$ cells.

E Age-associated changes in YBX1 levels in human BMSCs from 30 males (left panel) and 30 females (right panel).

F, G Representative images of Alizarin Red staining (F) and quantification of calcification (G) by detecting the amount of Alizarin Red extracted from the matrix in BMSCs transfected with adenovirus driven control and *Ybx1* shRNA at 21 days of osteogenic induction.

H, I Representative images of Oil Red O staining (H) and quantification of lipid formation by detecting the amount of Oil Red O extracted from the matrix (I) in BMSCs after 10 days of adipogenic induction.

J, K Representative images of β-Gal staining (J) and quantification (K) of β-Gal-positive cells among BMSCs.

L, M Relative mRNA levels of osteogenic differentiation related genes (L), adipogenic differentiation and senescence related genes (M) between BMSCs transfected with adenovirus driven control and *Ybx1* shRNA.

N Heat map of differentially expressed genes between BMSCs transfected with adenovirus driven control and *Ybx1* shRNA.

Data information: In (B), (D), (G), (I), and (K), $n = 5$ in each group from three independent experiments. In (L) and (M), $n = 3$ in each group from three independent experiments. In (N), $n = 3$ in each group. Data are shown as the mean ± SEM. Scale bar: 100 μm. *$P < 0.05$; **$P < 0.01$; ***$P < 0.001$; Student's *t*-test for (B), (D), (L), (M) and one-way ANOVA for (G), (I), (K).

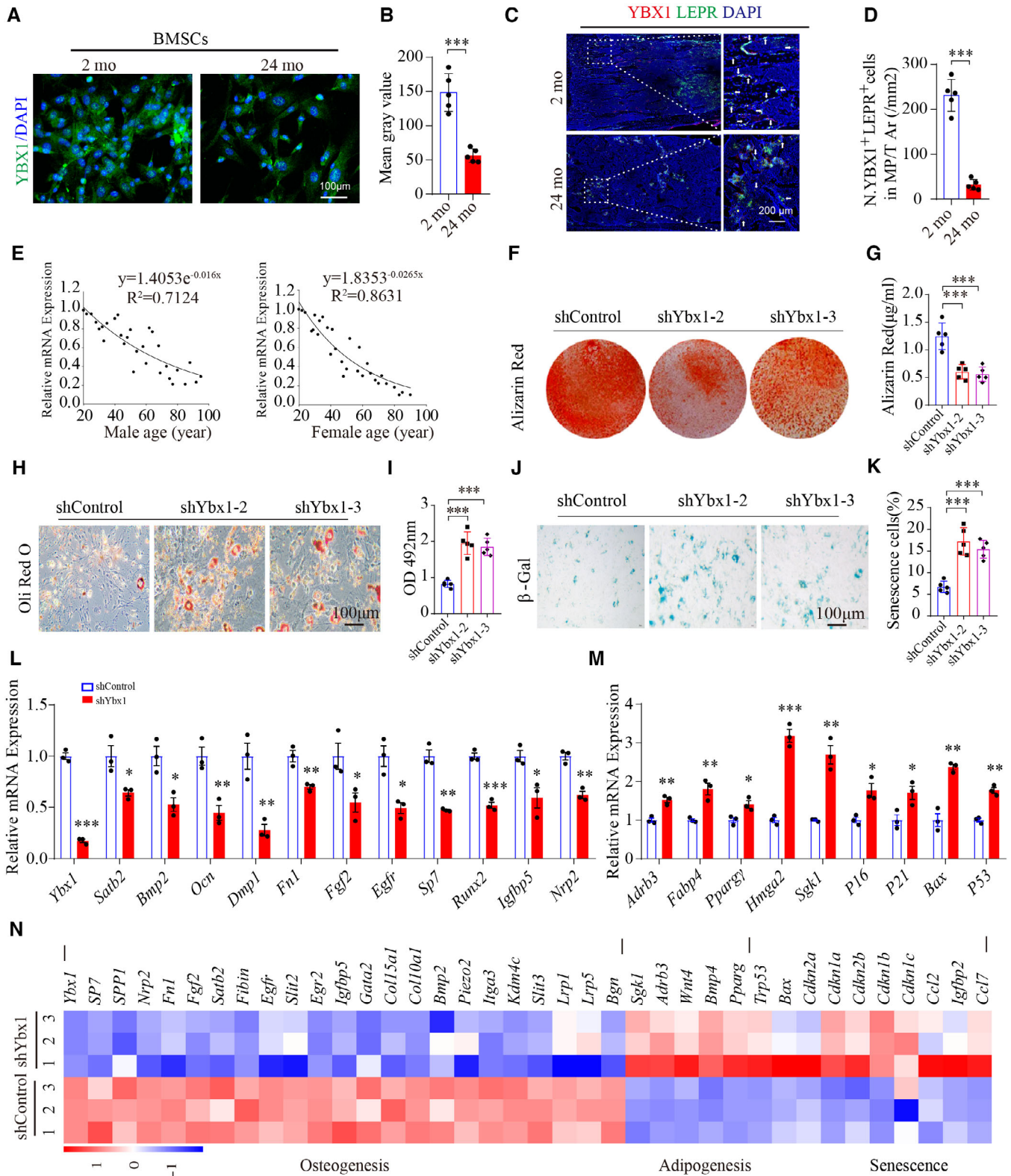Figure 2.

trabecular separation when compared with controls (Appendix Fig S3B–F). *Ybx1^{lepr-CKO}* mice also had significantly higher numbers of adipocytes in their bone marrow (Appendix Fig S3G and H), but

lower number of osteoblasts on the trabecular bone surfaces (Appendix Fig S3I and J). However, the number of osteoclasts on bone surfaces was unchanged (Appendix Fig S3K and L).
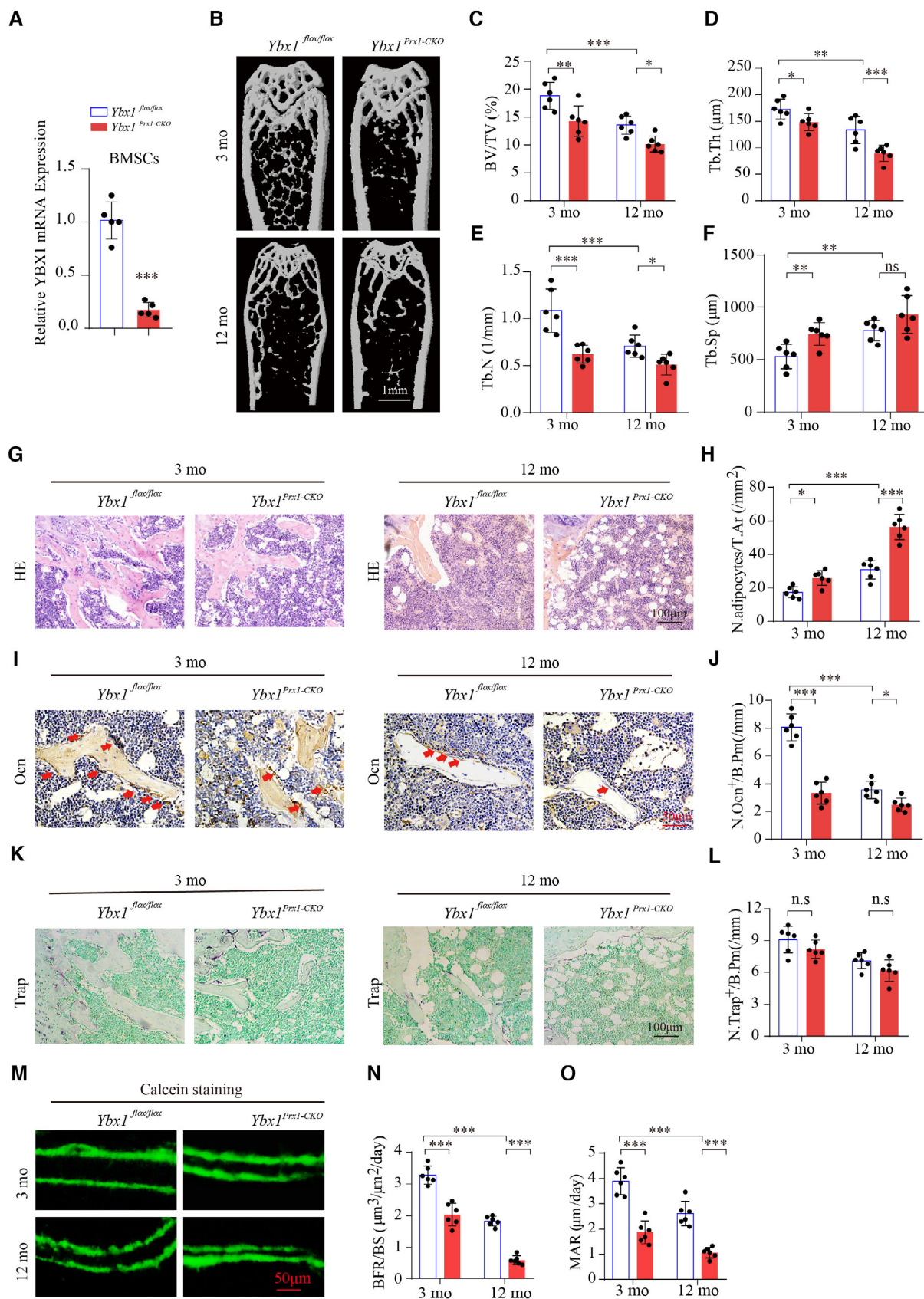
Figure 3.

Figure 3.   Depletion of YBX1 in BMSCs results in accelerated bone loss and bone marrow fat accumulation.

A   qRT-PCR analysis of the levels of *Ybx1* in BMSCs isolated from *Ybx1^Prx1-CKO* mice and *Ybx1^flox/flox* mice.

B–F   Representative µCT images, Scale bar: 1 mm. (B) and quantitative µCT analysis of trabecular bone microarchitecture (C–F) in distal femora from 3- and 12-month-old male *Ybx1^Prx1-CKO* mice and *Ybx1^flox/flox* mice (BV/TV, bone volume per tissue volume; Tb.N, trabecular number; Tb.Th, trabecular thickness; Tb.Sp, trabecular separation).

G   Representative images of H&E staining (Hematoxylin–Eosin Staining) in distal femora. Scale bar: 100 µm.

H   Quantification of the number of adipocytes related to the tissue area (N. adipocytes/T.Ar).

I   Representative images of osteocalcin (OCN) immunohistochemical staining in distal femora. Arrows point to osteocalcin positive cells. Scale bar: 50 µm.

J   Quantification of osteocalcin positive cells on the bone surface. Number of OCN$^+$ cells per bone perimeter (N. Ocn$^+$/B.Pm).

K   Representative images of TRAP staining in distal femora. Scale bar: 100 µm.

L   Quantification of TRAP positive cells on the bone surface. Number of TRAP$^+$ cells per bone perimeter (N. Trap$^+$/B.Pm).

M   Representative images of calcein double labeling of trabecular bone. Scale bar: 50 µm.

N   Quantification of the bone formation rate (BFR) based on calcein double labeling.

O   Quantification of the mineral apposition rate (MAR) based on calcein double labeling.

Data information: *n* = 6, biological replicates in each group. Data are shown as the mean ± SEM. n.s., no significant difference; *$P < 0.05$; **$P < 0.01$; ***$P < 0.001$; Student's *t*-test for (A), one-way ANOVA for (C), (D), (E), (F), (H), (J), (L), (N), and (O).

These results suggested that depletion of YBX1 accelerated bone loss and stimulated bone marrow fat accumulation.

Overexpression of *Ybx1* attenuated fat accumulation and promoted bone formation in aged mice

Next, we investigated whether elevating the level of YBX1 could attenuate the senescence of BMSCs and stimulate their osteogenic differentiation. We isolated BMSCs from 3-month-old mice and transfected them with a *Ybx1* overexpression plasmid. BMSCs overexpressing *Ybx1* showed enhanced osteogenic differentiation, as indicated by Alizarin Red staining (Fig 4A; Appendix Fig S6A) and restrained adipogenic differentiation, as indicated by Oil Red O staining (Fig 4B; Appendix Fig S6B). Overexpression of *Ybx1* also reduced BMSC senescence, as indicated by β-Gal staining (Fig 4C).

To investigate whether recovery of YBX1 expression could further alleviate age-associated bone loss *in vivo*, we constructed AAV serotype 8 with a CMV promoter for gene delivery of *Ybx1* (rAAV8-GFP-*Ybx1*) to overexpress YBX1 in BMSCs. We treated 23-month-old mice with rAAV8-GFP-*Ybx1* via intra-bone marrow injection. One month later, *Ybx1* mRNA levels in BMSCs isolated from femur

that was injected with rAAV8-GFP-*Ybx1* were much higher than those in the control (Fig 4D). In addition, µCT analysis showed a higher bone volume, trabecular number, and lower trabecular separation in *Ybx1* overexpressing femurs compared with those in the control group (Fig 4E and F). rAAV8-GFP-*Ybx1*-treated femurs had significantly lower bone marrow fat accumulation (Fig 4G and H) and more osteoblasts on the trabecular bone surfaces (Fig 4I and J); however, the number of osteoclasts on bone surfaces was unchanged (Fig 4K and L). Calcein double labeling revealed that rAAV8-GFP-*Ybx1*-treated femurs had a significantly higher trabecular bone MAR and BFR compared with those of the control (Fig 4M and N).

These results suggested that recovering YBX1 expression restrained age-related bone loss and bone marrow fat accumulation in old mice.

YBX1 regulated the fate of BMSCs by regulating the splicing of pre-mRNAs critical for differentiation and senescence

To further investigate the role of splicing factor YBX1 in BMSCs, we evaluated changes in pre-mRNA splicing between BMSCs isolated

Figure 4.   Overexpression of *Ybx1* attenuated fat accumulation and promoted bone formation in aged mice.

A   Representative images of Alizarin Red staining (left panel) and quantification of calcification (right panel) by detecting the amount of Alizarin Red extracted from the matrix in BMSCs transfected with the control or *Ybx1* plasmid at 21 days of osteogenic induction.

B   Representative images (left panel) and quantification (right panel) of Oil Red O staining in BMSCs transfected with the control or *Ybx1* plasmid at 10 days of adipogenic induction.

C   Representative images of β-Gal staining (left panel) and quantification (right panel) of β-Gal-positive cells in BMSCs transfected with the control or *Ybx1* plasmid.

D   qRT-PCR analysis of the expression of *Ybx1* in BMSCs from mice with rAAV8-GFP-*Ybx1* or rAAV8-GFP transfection.

E, F   Representative µCT images, Scale bar: 1 mm. (E) and quantitative µCT analysis of trabecular bone microarchitecture (F) in distal femora from 24-month-old mice with rAAV8-GFP-*Ybx1* or rAAV8-GFP transfection (BV/TV, bone volume per tissue volume; Tb.N, trabecular number; Tb.Th, trabecular thickness; Tb.Sp, trabecular separation).

G   Representative images of H&E staining in distal femora.

H   Quantification of the number of adipocytes related to the tissue area (N. adipocytes/T.Ar).

I   Representative images of osteocalcin immunohistochemical staining in distal femora. Arrows point to osteocalcin positive cells.

J   Quantification of osteocalcin positive cells in bone surface. Number of OCN$^+$ cells per bone perimeter (N. Ocn$^+$/B.Pm).

K   Representative images of TRAP staining in distal femora.

L   Quantification of TRAP positive cells on the bone surface. Number of TRAP$^+$ cells per bone perimeter (N. Trap$^+$/B.Pm).

M   Representative images of calcein double labeling of trabecular bone.

N   Quantification of the bone formation rate (BFR) and mineral apposition rate (MAR) based on calcein double labeling.

Data information: *n* = 6, biological replicates in each group. Data are shown as the mean ± SEM. Scale bar: 50 µm. n.s., no significant difference; *$P < 0.05$; **$P < 0.01$; ***$P < 0.001$; Student's *t*-test.
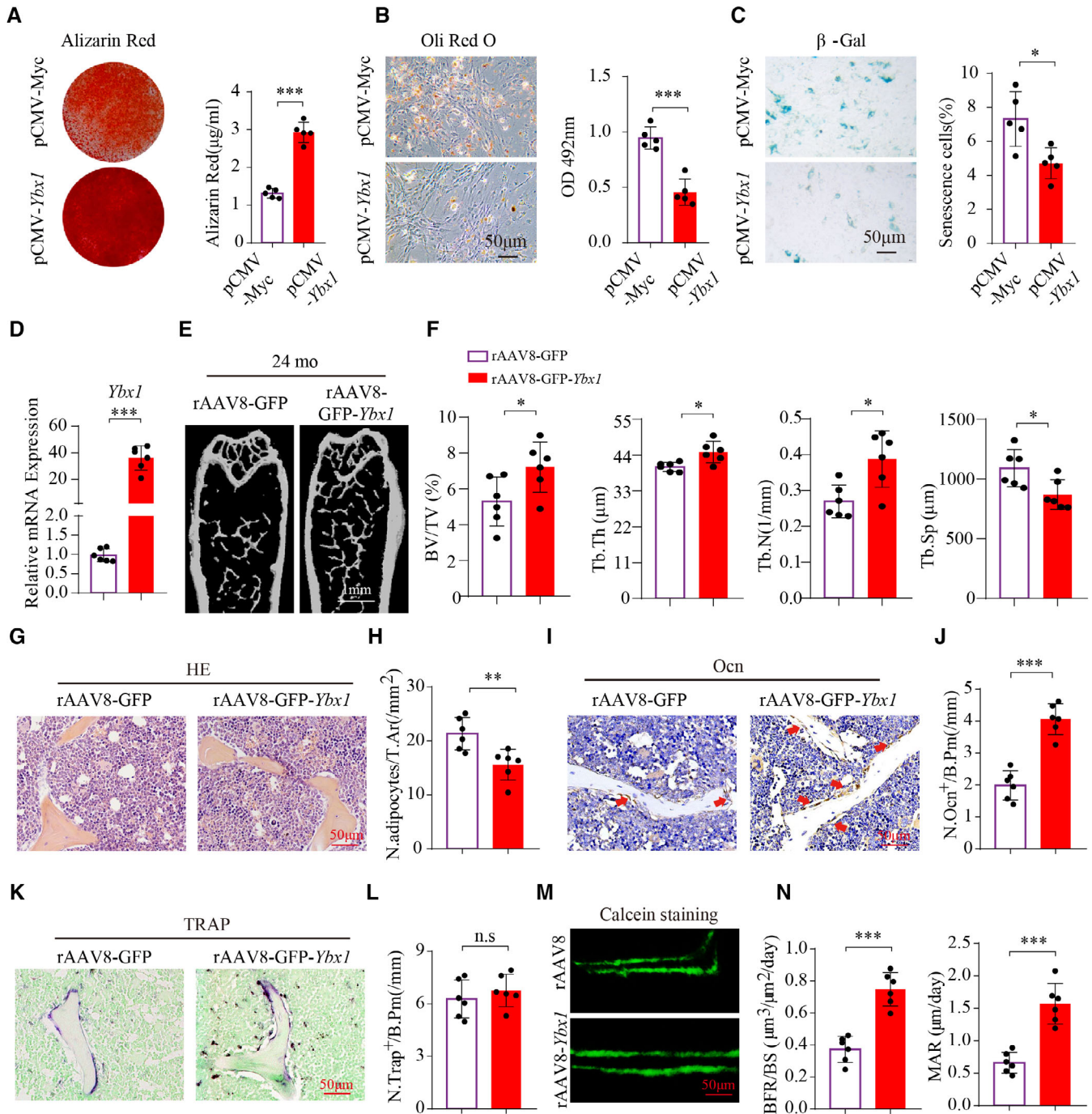
Figure 4.

from $Ybx1^{Prx1-CKO}$ mice and their $Ybx1^{flox/flox}$ littermate controls by calculating the ΔPSI values of major AS events (Appendix Fig S4A and B). There were 234 pre-mRNAs that showed AS with a ΔPSI > 0.1 and P-value < 0.05. The change in pre-mRNA splicing upon $Ybx1$ deletion comprised alternative first exons (45.53%), alternative 5′ splice sites (17.45%), exon skipping (13.62%), intron retention (10.21%), alternative 3′ splice sites (9.79%), and alternative last exons (3.4%) (Appendix Fig S4B). We next performed liquid chromatography tandem mass spectrometry (LC–MS/MS) following

immunoprecipitation in BMSCs to identify YBX1 interaction partners (Appendix Fig S4C). Proteomic network analysis showed that YBX1 interacted with a number of proteins related to ribosomes, ribosome biogenesis, and the spliceosome complex (Appendix Fig S4D and E). Protein correlation analysis indicated that YBX1 and its related proteins form a regulatory network whose functions are mainly enriched in various RNA metabolic processes, including spliceosome and ribonucleoprotein complex assembly, snRNA processing, alternative mRNA splicing, and RNA splicing (Appendix Fig S4E and

F). Among these YBX1 interaction partners, a cluster of ribonucleo-proteins, mRNA splicing factors, and ribosomal proteins were significantly enriched, participating in the spliceosome assembly reaction to form a mature mRNA (Shi, 2017; Jayavelu *et al*, 2020; Appendix Fig S4G and H), which also indicated the core role of splicing factor YBX1 in pre-mRNA altered splicing events.

To further investigate the mechanism by which splicing factor YBX1 regulates the differentiation and senescence of BMSCs, we identified genome-wide targets of YBX1 in BMSCs using anti-YBX1 cross linking immunoprecipitation-high throughput sequencing (CLIP-seq) analysis using a BMSC cell line (Appendix Fig S5A). CLIP-seq analysis identified 7,890 YBX1-binding sites, approximately 51.69% of which were distributed in exons (Appendix Fig S5B), with the known and novel overrepresented motifs (Appendix Fig S5C). By combining RNA sequencing and anti-YBX1 CLIP analysis, we identified 66 pre-mRNAs in BMSCs with YBX1-binding sites that showed alternative splicing upon *Ybx1* deletion (Fig 5A). Among those mRNAs, BMSC osteogenesis-related genes *Fn1*, *Sp7*, and *Spp1*, and BMSC senescence-related genes *Sirt2* and *Nrp2* were identified as direct YBX1-mRNA-binding targets. These genes underwent mis-splicing, including exon skipping of *Fn1*, *Nrp2*, *Sirt2*, *Sp7*, and *Spp1* (Fig 5B). We constructed an RNA map for YBX1-dependent splicing regulation and found that repression and activation-related binding occurred at almost completely different sites (Appendix Fig S5D). Semiquantitative PCR validated the exon skipping of *Fn1*, *Nrp2*, *Sp7*, and *Sirt2* in BMSCs isolated from $Ybx1^{Prx1-CKO}$ mice (Fig 5C). To further determine whether this mis-splicing would affect BMSC differentiation and senescence, we transfected the different mRNA isoforms of *Sp7*, *Spp1*, or *Sirt2* into BMSCs, which then underwent osteogenic, adipogenic, or senescence induction. The long isoform of *Sp7* mRNA (without skipping of exon2) had a better promotive effect on osteogenic differentiation in BMSCs (Fig 5D and E), the long isoform of *Spp1* mRNA (without skipping of exon 4) had a better promotive effect on osteogenic differentiation (Fig 5F and G) and a better suppressive effect on adipogenic differentiation in BMSCs (Fig 5H and I), and the long isoform of *Sirt2* mRNA (without skipping of exon 2) had a better suppressive effect on senescence of BMSCs (Fig 5J and K). BMSCs isolated from $YBX1^{Prx1-CKO}$ mice showed decreased osteogenic differentiation (Fig 5L–O; Appendix Fig S6C), and increased adipogenic

differentiation (Fig 5P and Q; Appendix Fig S6D) and senescence (Fig 5R and S), which could be rescued by supplementing with normal effector transcripts of *Sp7*, *Spp1*, and *Sirt2* (Fig 5L–S).

To evaluate whether those altered pre-mRNA splicing events would result in a variation in the protein level, we performed Western blotting and demonstrated decreased levels of FN1, NRP2, SPP1, and SP7, whose pre-mRNAs had a direct YBX1-mRNA binding target and went through mis-splicing, in BMSCs isolated from $Ybx1^{Prx1-CKO}$ mice (Appendix Fig S5E and F). Our previous research suggested that YBX1 could directly bind to the promoter and repress the expression of *P16* in hypothalamic neural stem cells (Xiao *et al*, 2020). We also detected decreased expression of RUNX2 and increased expression of P16 and PPARG in BMSCs isolated from $Ybx1^{Prx1-CKO}$ mice (Appendix Fig S5E and F).

As an RNA-binding protein, YBX1 could also bind to the promoter regions of genes and regulate their expression (Kotake *et al*, 2013; Zhang *et al*, 2020). To investigate whether YBX1 regulated the senescence and osteogenesis-related genes of BMSCs at the transcriptional level, we performed YBX1 chromatin immunoprecipitation sequencing (ChIP-seq) and found that only 2.69% of peaks were located at the promoter region (Appendix Fig S5G), and there was no significant difference between the enrichment of YBX1 and input at the transcription start sites (TSSs) (Appendix Fig S5H). Additionally, there was no significant binding of YBX1 to the promoter regions of *Fn1*, *Nrp2*, *Sp7*, *Sirt2*, and *Spp1* genes (Appendix Fig S5I–M).

Taken together, these results suggested that YBX1 regulated the expression level of osteogenic differentiation, adipogenic differentiation, and senescence-related genes in BMSCs by controlling pre-mRNA alternative splicing.

Sciadopitysin bound to and inhibited ubiquitin-mediated degradation of YBX1

To search for a potential therapeutic strategy to restrain the age-related debility of BMSCs by targeting YBX1, we performed molecular docking to screen natural small molecular compounds that interacted with mouse YBX1, as previously reported (Xiao *et al*, 2020). We chose nine top-ranked small molecules that were related to anti-oxidation, anti-inflammation, anti-aging and bone metabolism (Fig 6A). Among these

---

Figure 5. YBX1 regulated the fate of BMSCs through regulating the splicing of pre-mRNAs critical for differentiation and senescence.

A   Venn diagrams of overlapping genes targeted by YBX1 and that showed alternative splicing upon YBX1 deletion. CLIP, ultraviolet cross-linking immunoprecipitation.

B   CLIP-seq read coverage across *Fn1*, *Nrp2*, *Sp7*, *Sirt2*, and *Spp1* from BMSCs. The dotted line regions indicate the location of the exon skipping. ES, Exon Skipping.

C   Semiquantitative PCR showing the different isoforms of *Fn1*, *Nrp2*, *Sp7*, and *Sirt2* from BMSCs of $Ybx1^{Prx1-CKO}$ mice and $Ybx1^{flox/flox}$ mice.

D–G   Representative images of Alizarin Red staining (D and F) and quantification of calcification by detecting the amount of Alizarin Red extracted from the matrix (E and G) in BMSCs transfected with different isoforms of *Sp7* or different isoforms of *Spp1*.

H, I   Representative images (H) and quantification of Oil Red O staining (I) in BMSCs transfected with different isoforms of *Spp1* with 10 days of adipogenic induction.

J, K   Representative images of β-Gal staining (J) and quantification (K) of β-Gal-positive cells in BMSCs transfected with different isoforms of *Sirt2*.

L–S   BMSCs were isolated from $Ybx1^{Prx1-CKO}$ mice and $Ybx1^{flox/flox}$ mice, among them, the BMSCs from $Ybx1^{flox/flox}$ mice were transfected with the blank control, BMSCs from $Ybx1^{Prx1-CKO}$ mice were transfected with the blank control or different isoforms of the target genes. (L–O) Representative images of Alizarin Red staining (L and N) and quantification of calcification by detecting the amount of Alizarin Red extracted from the matrix (M and O). (P, Q) Representative images (P) and quantification of Oil Red O staining (Q) in BMSCs after 10 days of adipogenic induction. (R, S) Representative images of β-Gal staining (R) and quantification (S) of β-Gal-positive cells among BMSCs.

Data information: In (C), $n = 2$ in each group from three independent experiments. In (E), (G), (I), (K), (M), (O), (Q), and (S), $n = 5$ in each group from three independent experiments. Data are shown as the mean ± SEM. Scale bar: 100 μm. n.s., no significant difference; *$P < 0.05$; **$P < 0.01$; ***$P < 0.001$; one-way ANOVA. Source data are available online for this figure.
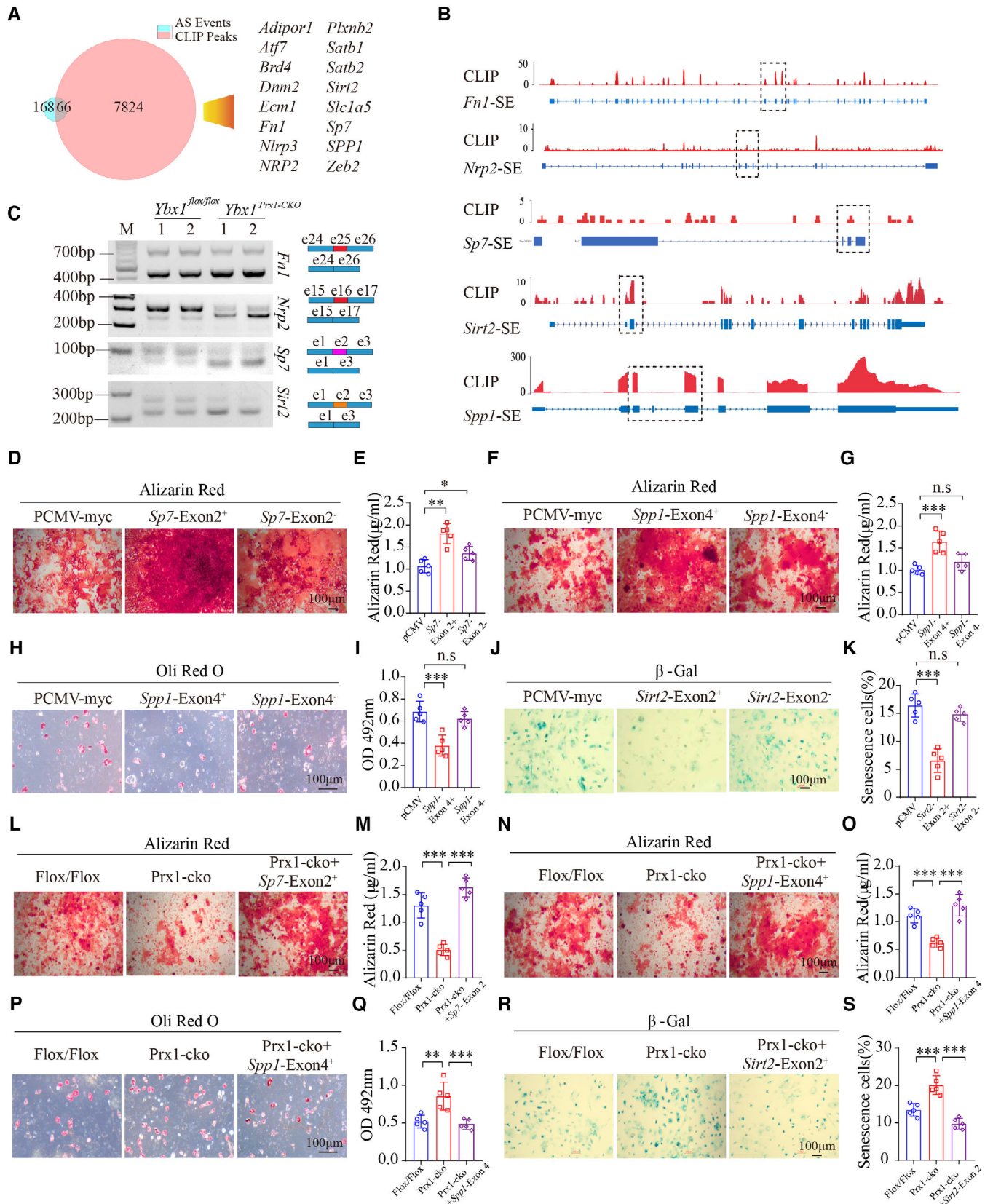
▶

Figure 5.

candidates, five compounds, including theaflavin-3-gallate, eriocitrin, sciadopitysin, isoginkgetin, and bilobetin, showed no adverse effect on BMSC proliferation, as evaluated using a Cell Counting Kit-8 (CCK8) assay (Fig 6B), and all five compounds had no effects on the transcription of *Ybx1* (Fig 6C). Only sciadopitysin and theaflavin-3-gallate could promote osteogenic differentiation, inhibit adipogenic differentiation, and attenuate the senescence of BMSCs, and between them, sciadopitysin showed better effects (Fig 6D–G; Appendix Fig S6E–G). Therefore, we chose sciadopitysin for further study. The structure and binding mode of sciadopitysin and YBX1 showed that sciadopitysin could enter into the pocket-like structure of YBX1 (Fig 6H). Sciadopitysin treatment increased the protein level of YBX1 in BMSCs (Fig 6I and M; Appendix Fig S6I). Sciadopitysin treatment could also increase the expression of *Fn1*, *Sirt2*, *Sp7*, and *Spp1* in BMSCs (Appendix Fig S7A–D). To investigate the means by which sciadopitysin treatment increased the protein level of YBX1, we blocked protein synthesis in BMSCs using cycloheximide (CHX) and found that sciadopitysin treatment slowed down the degradation of YBX1 (Fig 6I; Appendix Fig S6J). YBX1 was demonstrated to be degraded through ubiquitination (Lutz *et al*, 2006). Therefore, we further tested whether sciadopitysin treatment affected YBX1 ubiquitination and found that sciadopitysin significantly decreased the ubiquitination level of YBX1 (Fig 6J). Previous studies reported that ubiquitin ligase FBXO33 could bind to and mediate the ubiquitination of YBX1 (Lutz *et al*, 2006). To confirm the interaction between FBXO33 and YBX1, and investigate which region of YBX1 could bind to FBXO33, we generated a series of YBX1 plasmid mutants, transfected them into BMSCs, and performed co-immunoprecipitation (co-IP) assays. The results showed that deletion of the amino acids 128–322 (C-terminus) and the amino acids 42–53 (pocket area) of YBX1 impaired the interaction between YBX1 and FBXO33, suggesting that the C-terminus and the pocket area are crucial for YBX1 binding to FBXO33 (Fig 6K). We further confirmed the interaction between FBXO33 and YBX1 in BMSCs using an co-IP test, and the interaction was suppressed by sciadopitysin treatment (Fig 6L). Notably, sciadopitysin treatment could decrease the level of FBXO33 in BMSCs (Fig 6M; Appendix Fig S6H). These results suggested that sciadopitysin inhibits the ubiquitination-mediated degradation of YBX1 both by decreasing the level of ubiquitin ligase FBXO33 and by preventing YBX1 from combining with FBXO33. Furthermore, sciadopitysin treatment could also partially restrain the exon skipping of *Sirt2*, *Fn1*, and *Spp1* in

BMSCs isolated from 24-month-old mice (Fig 6N), which indicated that sciadopitysin could alleviate age-related mis-splicing of target genes in aged BMSCs.

Sciadopitysin treatment ameliorated age-related bone loss in mice

To further investigate whether sciadopitysin administration could alleviate age-related bone loss, 23-month-old C57/BL6J mice were administered with sciadopitysin at 40 mg/kg body weight per day or with vehicle for 2 months (Fig 7A). μCT analysis showed that the sciadopitysin-treated mice had a higher bone volume, trabecular thickness, and trabecular number, and lower trabecular separation compared with those of the vehicle treated mice (Fig 7B–F). Sciadopitysin-treated mice had significantly higher numbers of osteoblasts on the trabecular bone surfaces, compared with those of the vehicle-treated mice (Fig 7G and H). The number of adipocytes was also decreased by treatment with sciadopitysin (Fig 7I and J). However, the number of osteoclasts was not affected by sciadopitysin treatment (Fig 7K and L). Moreover, calcein double labeling analysis showed that sciadopitysin-treated mice had a significantly higher trabecular bone MAR and BFR compared with that of the vehicle-treated mice (Fig 7M–O). These results suggested that old mice treated with sciadopitysin experienced increased bone formation.

Taken together, we demonstrated that RNA-binding protein YBX1 can stimulate osteogenic differentiation and restrain the senescence of BMSCs by regulating a cluster of genes including *Fn1*, *Nrp2*, *Sirt2*, *Sp7*, and *Spp1* as a splicing factor. The decreased expression level of YBX1 during aging contributes to the debility of BMSCs, including increased senescence and reduced osteogenesis. Moreover, we identified a natural small compound, sciadopitysin, which could delay the degradation of YBX1 and attenuate age-related bone loss (Fig 7P).

Discussion

Age-related dysfunction of BMSCs, such as lineage switching between osteogenic and adipogenic fates, and acceleration of

---

Figure 6. Sciadopitysin bound to and inhibited ubiquitin degradation of YBX1.

A The homology modeling structure of mouse YBX1 and nine top-ranked candidates.

B Cell proliferation rate assessed using a CCK8 assay after administration of different compounds.

C qRT-PCR analysis of *Ybx1* expression in BMSCs after administration of different compounds.

D Representative images of Alizarin Red staining (up panel), Oil Red O staining (middle panel, scale bar: 100 μm) and β-Gal staining (bottom panel, scale bar: 100 μm) in BMSCs treated with different compounds.

E–G Quantification of calcium mineralization based on Alizarin Red staining (E), quantification of Oil Red O based on Oil Red O staining (F), and quantification of β-Gal-positive cells based on β-Gal staining in BMSCs treated with different compounds (G).

H The molecular structure of sciadopitysin and a model of the interaction between sciadopitysin and mouse YBX1.

I Western blotting analysis of YBX1 in sciadopitysin pretreated BMSCs after cycloheximide (CHX) treatment.

J Western blotting analysis of YBX1 related ubiquitination in sciadopitysin pretreated BMSCs administered with MG132.

K Co-IP of His-FBXO33 with HA-YBX1 and a series of mutant HA-YBX1 proteins following transfection into BMSCs.

L Co-IP of FBXO33 withYBX1 with or without the administration of sciadopitysin.

M Western blotting analysis of FBXO33 and YBX1 levels in BMSCs treated with different concentrations of sciadopitysin.

N Semiquantitative PCR showed the isoforms of *Fn1*, *Nrp2* and *Sirt2* in cultured BMSCs isolated from 2- or 24-month-old mice then treated with or without sciadopitysin.

Data information: In (B), (C), (E), (F), and (G), $n = 5$ in each group from three independent experiments. (I–N) is representative of three independent experiments. Data are shown as the mean ± SEM. n.s., no significant difference; *$P < 0.05$; **$P < 0.01$; ***$P < 0.001$; one-way ANOVA.
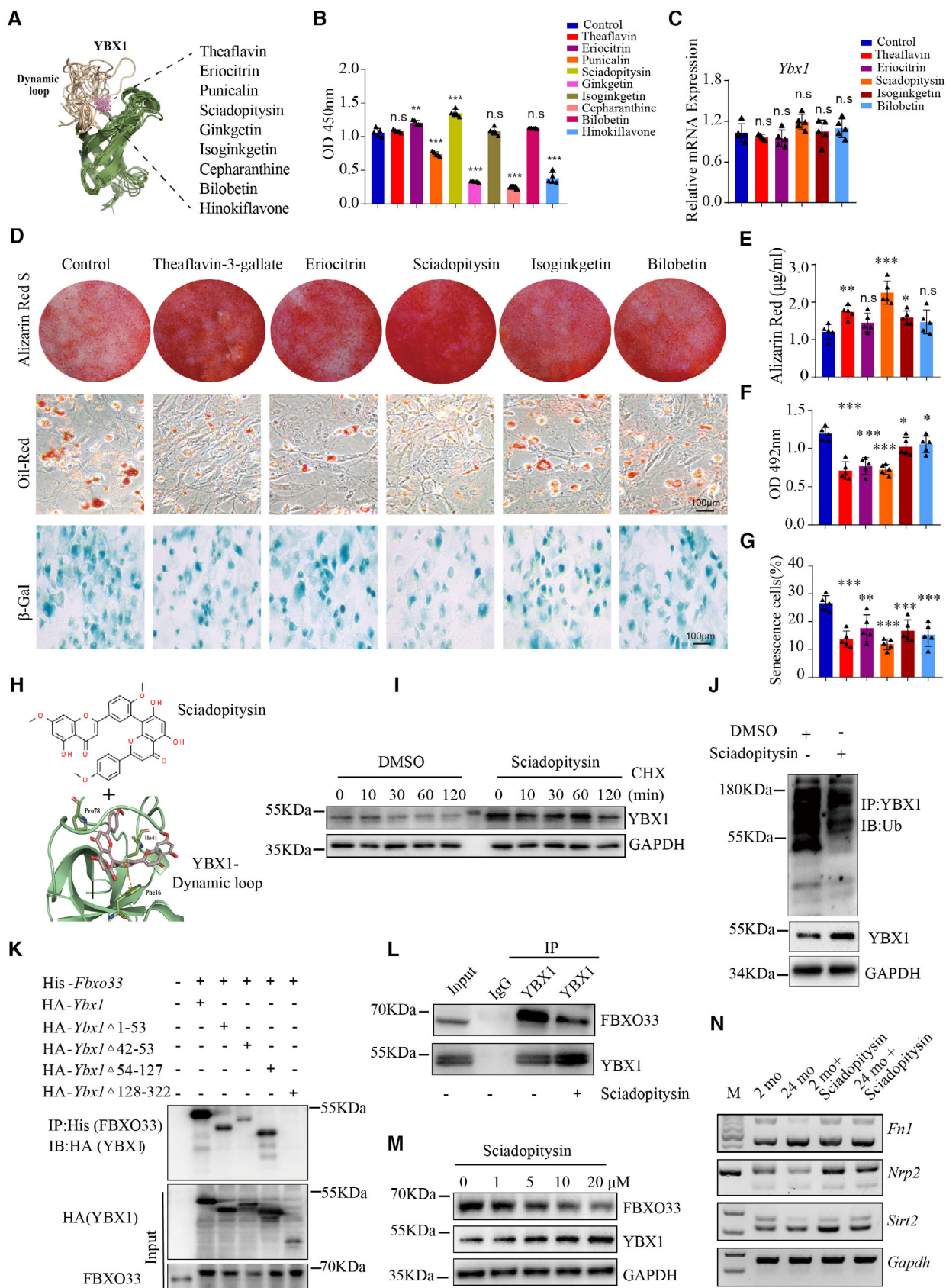Source data are available online for this figure.
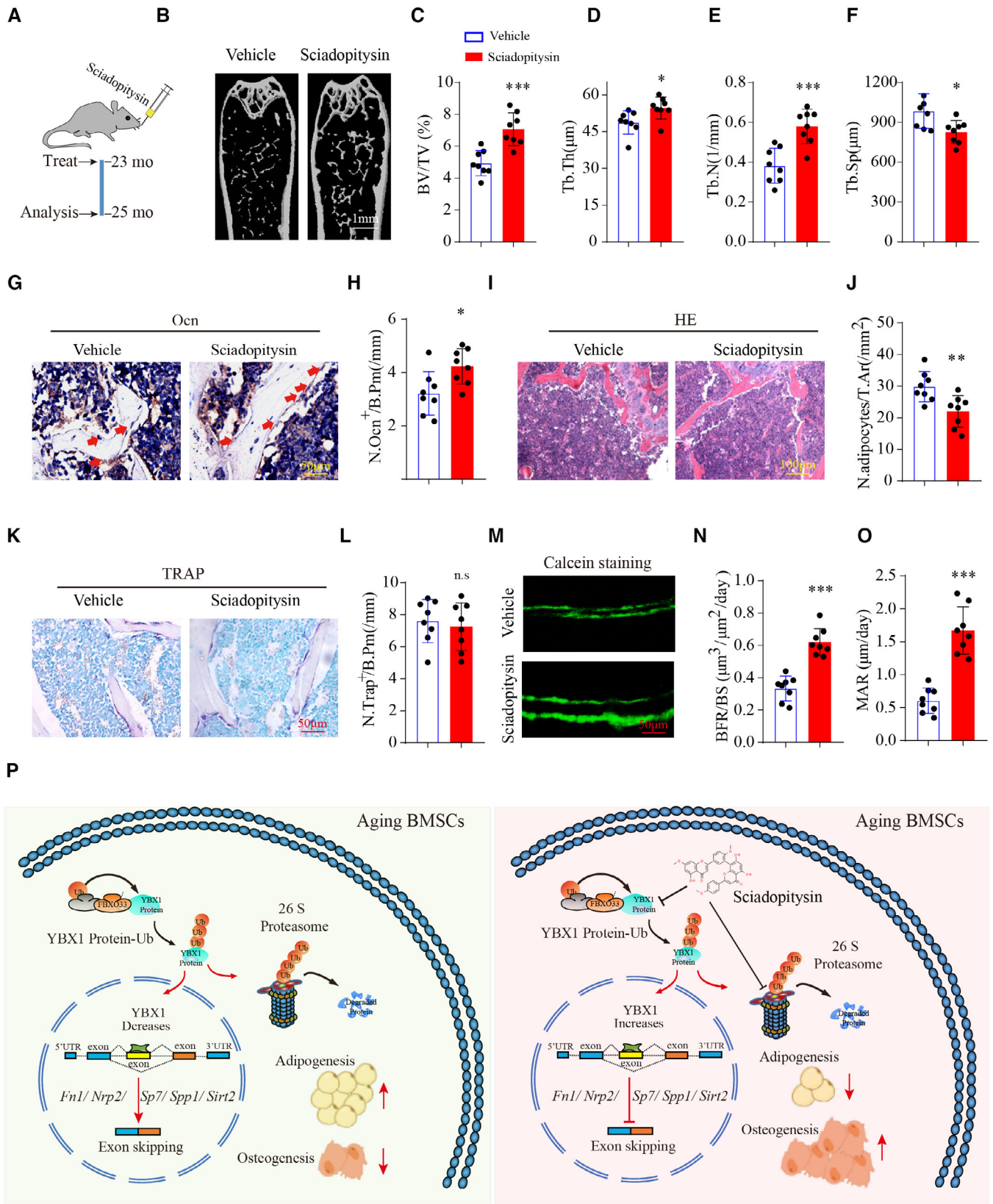
Figure 6.

Figure 7.

Figure 7. Sciadopitysin treatment alleviated aging-related bone loss in mice.

A   Schematic of the time of oral treatment of sciadopitysin in mice.

B–F   Representative μCT images, Scale bar: 1 mm. (B) and quantitative analysis of trabecular bone microarchitecture (C–F) in distal femora of 25-month-old mice administered with sciadopitysin or vehicle (BV/TV, bone volume per tissue volume; Tb.N, trabecular number; Tb.Th, trabecular thickness; Tb.Sp, trabecular separation).

G, H   Representative images (G) and quantification (H) of osteocalcin (OCN)-positive cells in distal femora of 25-month-old mice administered with sciadopitysin or vehicle. Number of Ocn$^+$ cells per bone perimeter (N. Ocn$^+$/B.Pm). Arrows point to osteocalcin positive cells. Scale bar: 50 μm.

I, J   Representative images (I) of H&E staining in distal femora and quantification (J) of the number of adipocytes related to the tissue area (right panel, N. adipocytes/T.Ar) in distal femora of 25-month-old mice administered with sciadopitysin or vehicle. Scale bar: 100 μm.

K, L   Representative images (K) and quantification (L) of TRAP-positive cells in distal femora of 25-month-old mice administered with sciadopitysin or vehicle. Number of TRAP$^+$ cells per bone perimeter (N. Trap$^+$/B.Pm). Scale bar: 50 μm.

M   Representative images of calcein double labeling of trabecular bone. Scale bar: 50 μm.

N, O   Quantification of the bone formation rate (BFR, N) and mineral apposition rate (MAR, O) based on calcein double labeling.

P   RNA binding protein YBX1 regulates a cluster of genes including *Fn1*, *Nrp2*, *Spp1*, *Sirt2* and *Sp7* as a splicing factor in the nucleus, which further stimulates osteogenic differentiation and restrains the senescence of BMSCs. The decreased expression level of YBX1 during aging contributes to the debility of BMSCs, including increased senescence and reduced osteogenesis. Sciadopitysin can delay the ubiquitination degradation of YBX1 by preventing YBX1 from binding to ubiquitin ligase FBXO33 (model based on data from previous figures).

Data information: $n = 8$, biological replicates in each group. Data are shown as the mean ± SEM. n.s., no significant difference; *$P < 0.05$; **$P < 0.01$; ***$P < 0.001$; Student's t-test.

senescence are critical in age-associated osteoporosis. Alternative splicing, as an important regulatory pathway of gene expression, has a wide range of biological functions. Disruption of alternative splicing can lead to dysfunction or disease (Fan & Tang, 2013). Aberrant alternative splicing can accelerate cellular senescence (Maier *et al*, 2004), and disrupt the differentiation of mesenchymal stem cells (Milona *et al*, 2003; Makita *et al*, 2008; Aprile *et al*, 2018). It has been reported that MSCs from old and young donors have different alternative splicing events (Peffers *et al*, 2016). However, whether aberrant alternative splicing participates in aging-related dysfunction of BMSCs, and its mechanism, remains unclear. In the present study, we observed altered splicing events and changed gene expression pattern in mouse BMSCs during aging using full-length transcriptome sequencing analysis and alternative splicing analysis. We further demonstrated that deficiency of the splicing factor YBX1 was responsible for mis-splicing of BMSCs fate-related genes and further resulted in senescence and a change in the differentiation direction of aged BMSCs.

As a well-known transcriptional and translational regulator, YBX1 participates in a variety of RNA-dependent events, including pre-mRNA transcription and splicing, mRNA packaging, mRNA stability, and translation (Eliseeva *et al*, 2011; Shah *et al*, 2021). At the cell level, the activities of YBX1 are involved in the regulation of multiple processes of cellular biology, such as cell proliferation, differentiation, stress response, and malignant cell transformation (Evans *et al*, 2020; Jayavelu *et al*, 2020; Zhang *et al*, 2020; Shah *et al*, 2021). In this study, we found that the expression level of YBX1 in BMSCs was decreased during aging, and further demonstrated that BMSC osteogenesis-related genes *Fn1*, *Spp1*, and *Sp7*, and senescence-related gene *Sirt2*, were identified as direct YBX1-mRNA-binding targets that underwent altered splicing. As a multifunctional RNA-binding protein, YBX1 not only acts as a splicing factor, but also has other functions that regulates BMSC fate decisions. Our previous research suggested that YBX1 could directly bind to the promoter and repress the expression of *P16*, thus controlling the senescence of hypothalamic neural stem cells (Xiao *et al*, 2020). In this study, analysis of CLIP-seq data showed that YBX1 has a binding peak in the exon2 region of *p16*. Unfortunately, the rPSI value was not significant in the *Ybx1*$^{Prx1-CKO}$ group

compared with that in the control group. Interestingly, Western blotting showed that deletion of *Ybx1* increased P16 levels in BMSCs, which indicated that YBX1 might regulate the expression of *p16* via an indirect pathway. We also identified 89 mRNAs in BMSCs, including several osteogenesis-related genes and senescence-related genes with YBX1-biding sites in their 3′ UTR regions, which showed altered expression upon *Ybx1* deletion. These results suggested that beside pre-mRNA alternative splicing, YBX1 might also regulate BMSC fate decisions by directly regulating the transcription of specific genes or maintaining the stability of mRNAs. Our study demonstrates that YBX1 is involved in the regulation of BMSC fate decisions during aging, and pre-mRNA alternative splicing is one of the important regulatory pathways.

Through further research, we found that BMSC-specific *Ybx1* knockout mice had accelerated bone loss and bone marrow fat accumulation compared with the control mice. In addition, overexpression of *Ybx1* in bone marrow using rAAV8-GFP-YBX1 attenuated bone loss and bone marrow fat accumulation, which further confirmed that YBX1 is a critical factor in orchestrating lineage commitment of BMSCs during aging. Our findings indicated that restoring the level of YBX1 in BMSCs during aging might be a therapeutic strategy to alleviate age-associated osteoporosis.

Sciadopitysin is an amentoflanove-type biflavonoid derived from *Taxus chinensis*. Choi's research group using the MC3T3-E1 cell line, demonstrated that sciadopitysin protects osteoblast function via upregulation of mitochondrial biogenesis (Suh *et al*, 2013; Choi *et al*, 2014). In our study, we identified that sciadopitysin could bind to YBX1 to attenuate its ubiquitination-mediated degradation, and further increased osteogenic differentiation and inhibited the senescence of BMSCs. Treatment with sciadopitysin could attenuate age-related bone loss in mice and could partially restrain the exon skipping of *Sirt2*, *Sp7*, and *Spp1* in BMSCs isolated from aged mice. All these results indicated that sciadopitysin exerts its protective effect on bone mass partly through YBX1. In this study, we did not investigate other mechanisms involved and thus could not exclude the effect of sciadopitysin outside of YBX1. Moreover, the efficacy and safety of sciadopitysin requires further evaluation in larger animals. We believe that sciadopitysin could be a major candidate compound to design new anti-osteoporosis drugs.

Taken together, the results of the present study demonstrated that YBX1 functions as an alternative splicing factor to regulate BMSC senescence and fate decisions and could be a potential therapeutic target for the treatment of age-related osteoporosis.

Materials and Methods

Animals

$Ybx1^{flox/+}$ mice were purchased from Cyagen Biosciences. *Prx1-Cre* transgenic mice and *Lepr-Cre* transgenic mice were purchased from the Jackson Laboratory. We mated $Ybx1^{flox/+}$ male mice with $Ybx1^{flox/+}$ female mice to obtain $Ybx1^{flox/flox}$ mice. We crossed *Prx1-Cre* mice or *Lepr-Cre* transgenic mice with $Ybx1^{flox/flox}$ to obtain *Prx1-Cre; $Ybx1^{flox/flox}$* or *Lepr-Cre; $Ybx1^{flox/flox}$* mice as homozygous conditional *Ybx1* knockout mice. The littermate $Ybx1^{flox/flox}$ mice were used as controls.

All the mice used in this study were bred under specific-pathogen-free conditions of Laboratory Animal Research Center at Central South University. All the mice were kept in a C57BL/6 background. All animal care protocols and experiments were approved by the Medical Ethics Committee of Xiangya Hospital of Central South University. Approval number: 2019030350.

Intra-bone marrow injection of adeno-associated virus

Intra-bone marrow delivery of virus was performed as previous reported (Li *et al*, 2018). Recombinant adeno-associated serotype 8 virus with CMV promoter for YBX1 overexpression (rAAV8-GFP-*Ybx1*) was purchased from Hanbio Biotechnology Co (Shanghai, China). The virus was diluted with sterile 1× PBS, and the viral titer used in the study was 5×10^{12} vg/ml. We used rAAV8-GFP as control. Five microliters of either rAAV8-GFP-*Ybx1* or rAAV8-GFP was delivered into the femoral medullary cavity through periosteal injection twice a month for 1 month.

Compound treatment

Sciadopitysin (T5S2129), Eriocitrin (T6S0221), Isoginkgetin (T4S21320), Bilobetin (T4S2128), Theaflavin3-gallate (T3051), Punicalin (T4S1718), Ginkgetin (T4S2126), Cepharanthine (T0131), and Hinokiflavone (T4S0181) were purchased from TargetMol. For *in vivo* studies, sciadopitysin was treated by oral gavage at 40 mg/kg body weight/day for 2 months. For *in vitro* experiment, sciadopitysin, eriocitrin, isoginkgetin, bilobetin, theaflavin3-gallate, punicalin, ginkgetin, cepharanthine, and hinokiflavone were dissolved in DMSO and treated at the concentration of 10 μM unless specified otherwise.

Primary mouse BMSC isolation and culture

Primary mouse BMSCs were isolated as previously reported (Li *et al*, 2015). We flushed bone marrow cells from the tibia and femora of male mice and incubated the cells with anti-Sca-1-PE (108108; BioLegend), anti-CD29-FITC (102206; BioLegend), anti-CD45-PerCP (103132; BioLegend), and CD11b-PerCP (101226; BioLegend) for 20 min at 4°C. For human BMSCs, human bone marrow cells were collected and incubated with FITC-, APC-, and PE-conjugated antibodies that recognized human Stro-1 (BioLegend, 340106), CD45 (BioLegend, 304012), and CD146 (BioLegend, 361008) at 4°C for 30 min. The acquisition was conducted on a fluorescence-activated cell sorting (FACS) Aria model (BD Biosciences). FACS DIVE software version 6.1.3 (BD Biosciences) was used for the analysis.

The sorted mouse Sca-1$^+$CD29$^+$CD45$^-$CD11b$^-$ BMSCs and human CD146$^+$Stro-1$^+$CD45$^-$ BMSCs were cultured for about 1 week to reach 80–85% confluence. Then, first-passage BMSCs were digested with trypsin for about 1 min and seeded in culture dishes for the enrichment of cell populations.

Cell culture, transfection, differentiation, and senescence assay

Bone marrow stromal cells were cultured in α-MEM supplemented with 10% fetal bovine serum (Gibco), 100 μg/ml streptomycin (Gibco), and 100 units/ml penicillin (Gibco) at 37°C with a humidified atmosphere of 5% CO_2. The BMSCs cell line we used was purchased from Cyagen (MUBMX-01001) and has been authenticated by STR profiling. Cell culture dishes and plates were purchased from NEST Biotechnology.

For YBX1 knockdown, adenovirus particles of shYBX1 and shControl were obtained from Hanbio Biotechnology Co (Shanghai, China). Bone marrow stromal cells were infected with adenovirus for 8 h before proceeding to perform further experiments. For YBX1 overexpression, mYBX1-Myc was purchased from Sino Biological Inc (MG51594-CM). The mYBX1 plasmid and negative control were transfected into BMSCs using Lipofectamine 2000 (Invitrogen) for 6 h before proceeding to perform further experiments.

For osteogenic differentiation assay, BMSCs were cultured in six-well plates at a density of 1.0×10^6 cells per well with osteogenic induction medium (10 mM β-glycerol phosphate, 0.1 μM dexamethasone, and 50 μM ascorbate-2-phosphate) for 3 weeks. Then, we stained the cells with 2% Alizarin Red (Cyagen Biosciences) to detect the cell matrix calcification. Alizarin Red was extracted from the matrix with cetyl-pyridinium chloride solution and quantified using spectrophotometry at 562 nm.

For adipogenic differentiation assay, BMSCs were plated in six-well plates at a density of 2.5×10^6 cells per well with adipogenic induction medium (1 μM dexamethasone, 5 μg/ml insulin, and 0.5 mM 3-isobutyl-1-methylxanthine) for 10 days. Culture medium was changed every 3 days. Lipid droplets in mature adipocytes were detected by Oil Red O staining according to the manufacturer's instruction (Cyagen Biosciences). Oil Red O was extracted from the matrix and quantified using spectrophotometry at 492 nm.

For cellular senescence assay, BMSCs were seeded in six-well plates at a density of 1.0×10^6 cells per well for 24 h. Senescent cells were stained using a β-Gal staining kit (Solarbio Science Technology) according to the manufacture' instructions.

Histochemistry analysis

Histochemistry analysis was performed as previously described (Li *et al*, 2015, 2018). Briefly, after the mice were euthanized, bones were harvested, fixed in 4% paraformaldehyde (PFA) for 24 h at 4°C, decalcified in 10% EDTA for 3 weeks at 4°C, and embedded in paraffin. 4-μm-thick longitudinal bone sections were made and

stained with TRAP (Sigma-Aldrich) and HE (Servicebio) according to the manufacturer's instructions.

Immunohistochemical staining

Immunohistochemical staining was performed as previously reported (Yang *et al*, 2017). Briefly, after antigen retrieval, bone sections were blocked in 5% bovine serum albumin (BSA) for 1 h at room temperature and incubated with primary antibody to osteocalcin (Takara, M173) at 4°C overnight. Then, the bone sections were incubated with appropriate secondary antibody at room temperature for 1 h. Finally, we detected the immunoactivity with an HRP-streptavidin detection system (Dako), and counterstained the slides with hematoxylin.

Calcein double-labeling assay

To evaluate dynamic bone formation ability, mice were administrated intraperitoneally with calcein (25 mg/kg, SigmaAldrich) at 8 and 2 days before euthanasia. After fixation in 70% ethanol, the samples were dehydrated in gradient ethanol. Then, the calcein double labeled bones were embedded in methyl methacrylate. 5-μm-thick longitudinal bone sections were made using a microtome and observed under a fluorescent microscope. Bone formation rate (BFR) and mineral apposition rate (MAR) were measured using the OsteoMeasureXP Software (Osteo-Metrics, Inc.). MAR and BFR can be measured directly. MAR: the rate of formation of mineralized layer on the surface of trabecular bone, which is calculated by dividing the distance between two markers by the interval time between markers. BFR: The length of the tetracycline labels (mineralizing surface per bone surface [MS/BS]) multiplied by the distance between labels (MAR) is the area of new bone formed during the label interval, thus BFR = MS/BS × MAR (Ott, 2008).

Immunofluorescence staining

Cultured BMSCs were fixed with 4% PFA for 15 min at room temperature. Then, the cells were blocked with 5%BSA for 1 h at room temperature, and incubated with YBX1 antibody (Cell Signaling Technology, 4202S, 1:100) over night at 4°C. After that, the cells were incubated with Alexa 488 (Invitrogen, A21106) and Alexa 555 (Invitrogen, A21422) conjugated secondary antibodies and the nucleus were stained with DAPI.

For bone sections, after antigen retrieval, bone sections were blocked with 5% BSA for 1 h at room temperature. Then, the bone sections were incubated with YBX1 antibody (Santa Cruz Biotechnology, sc-398340, 1:100), LEPR Polyclonal antibody (Proteintech, 20966-1-AP, 1:100) over night at 4°C. Next, the bone sections were incubated with Alexa 488 (Invitrogen, A21106) and Alexa 555 (Invitrogen, A21422) conjugated secondary antibodies and the nuclear were stained with DAPI.

qRT-PCR analysis

Total RNA was extracted with RNAex Pro RNA reagent (Accurate Biotechnology (Hunan) Co., Ltd) and RNA purity and concentration was determined by BioTek Epoch2 microplate reader (BioTek, USA). Total RNA (1 μg) was reversed with Evo M-MLV RT Kit with gDNA Clean for qPCR AG11705 (Accurate Biotechnology (Hunan) Co., Ltd). Quantitatification of mRNA was detected by qRT-PCR with SYBR® Green Premix Pro Taq HS AG11702 (Accurate Biotechnology (Hunan) Co., Ltd) for 40 cycles at 95°C for 3 s, 60°C for 30 s in ABI QuantStudio3 (Applied Biosystems). The relative quantitation value for each target gene was given by $2^{-\Delta\Delta C_t}$ method using Gapdh as an internal control. Primers for qPCR were shown in Appendix Table S1.

RNA sequencing

The total RNA from BMSCs cell line infected with shYBX1 or shControl adenovirus and BMSCs isolated from 2-month, 24-month, Ybx1^flox/flox^, and Ybx1^Prx1-CKO^ mice was extracted with RNAex Pro RNA reagent, and then assessed by Agilent 2100 Bioanalyzer (Agilent Technologies, Waldbronn, Germany). The cDNA libraries were produced by NEB Next® UltraTM RNA Library Prep Kit for Illumina® (NEB, USA) and then arrayed for high-throughput sequencing with Illumina NovaSeq6000 platform. Raw reads were cleaned by removing low-quality reads and adapter sequences. The clean data were mapped to the reference genome using Hisat2 v2.0.5. The DESeq2 R package (1.16.1) was used to perform differential expression analysis of two groups. The gene expression is considered to be significantly different if displaying ≥ 1.3-fold change and *P*-value < 0.05.

PacBio Iso-Sequencing and alternative splicing analysis

The total RNA from BMSCs isolated from 2-month, 24-month, Ybx1^flox/flox^, and Ybx1^Prx1-CKO^ mice was extracted and reversed to cDNA with SMARTer PCR cDNA Synthesis Kit (Clontech, UK), followed by PCR amplification with KAPA HiFi PCR Kits and selected by BluePippin Size Selection System (samples > 4 kb) as defined by Pacific Biosciences. The size-selected amplification products subsequently were produced to SMRTbell libraries using SMRTbell template prep kit 1.0 (PacBio, USA). Sequencing was performed on the PacBio Sequel II platform (Annoroad Gene Tech. (Beijing) Co., Ltd). QC of raw reads was performed using SMRT Link Portal v9.0, with subsequent analysis using the Iso-Seq3.1.2 pipeline to obtain High-quality, full-length transcripts. Iso-Seq isoform expression was determined from alignment of RNA-Seq reads to Iso-Seq isoforms, generated from Cupcake scripts, using Kallisto. Alternative splicing (AS) events were analyzed using AStalavista. Differential alternative splice of two conditions was estimated using PSI-Sigma. A significantly differential splicing event is reported only when it has more than 10% PSI change in the comparison and has a *P*-value lower than 0.05. Seven major AS events, namely exon skipping, intron retention, alternative first exon, alternative last exon, alternative 5′ splice site, alternative 3′ splice site, and mutually exclusive exon, were extracted from the output files and counted, respectively (Xia *et al*, 2017).

Cross- linking immunprecipitation (CLIP) sequencing and data analysis

Bone marrow stromal cells (1 × 10⁸ cells) were treated with 4-thiouridine (100 μM) for 16 h. After 16-h incubation, cells were washed twice with 10 ml of ice-cold PBS and then were UV

irradiated at 150 mj/cm^2 on ice. Cells were collected with a clear cell scraper and transferred into a new 15-ml centrifuge tube and then pelleted at 1,000 *g* for 5 min at 4°C. The supernatant was discarded, and the cell pellet was resuspended with 12 ml 1× cell lysis buffer containing 120 μl 100× DTT and 120 μl 100× Protease inhibitor and incubated on ice for 10 min. Cell lysates were centrifuged at 14,000 *g* for 15 min at 4°C and transfered supernatant into a new 15-ml centrifuge tube. For CLIP procedure, 8 ml of supernatant was incubated with 5 μg YBX1 antibody (Cell Signaling Technology, 9744S), and 4 ml of supernatant was incubated with 2 μg IgG antibody overnight at 4°C. The next day, CLIP samples were further incubated with 40 μl ProteinA/G magnetic beads for 3 h at 4°C. The magnetic beads were washed twice with 1× IP wash buffer and subsequently resuspended in 60 μl 1× IP wash buffer containing 6 μl RNase T1. The magnetic beads were incubated at 22°C for 60 min and at ice for 5 min and then washed twice with 1× IP wash buffer. Next, the magnetic beads were resuspended in 100 μl 1× IP wash buffer containing 20 μl DNase I and incubated at 37°C for 15 min and at ice for 5 min. The beads were placed on the magnetic separator then washed twice with 1× IP wash buffer. Finally, the magnetic beads were resuspended in 1 × 100 μl Proteinase K and incubated at 55°C for 30 min. To remove the beads by a magnetic separator, transfer the supernatant into a new 1.5-ml centrifuge tube. An equal volume acidic phenol: chloroform: isoamylalcohol (25:24:1) and equal volume chloroform was used to clear the supernatant. After, the clear supernatant was added with 2 volumes of ethanol and 1 μl of glycogen and then precipitated at −20°C for 2 h. The supernatant was centrifuge at 14,000 rpm for 30 min at 4°C and discarded the supernatant. The precipitate was washed twice with 75% ethanol and resuspended with 10 μl RNase-free water. The recovered RNA was used to perform the high-throughput sequencing with Illumina NovaSeq6000 system under the help of ABLife Inc and Wuhan Igenebook Biotechnology Co., Ltd. We performed the analysis of the CLIP data similarly as described previously (Wang *et al*, 2019). Briefly, the raw data were performed to filter out low-quality reads. Clean reads were mapped to the GRCm38.p6 genome with Hisat2 (Kim *et al*, 2015), to obtain the unique comparison on the genome, and remove the comparison result of PCR duplicate. Two software programs, Piranha and ABLIRC, to perform CLIP-seq peaks calling. Piranha has been reported previously (Uren *et al*, 2012). The "ABLIRC" strategy for peak calling was conducted for each IP sample, respectively (Xia *et al*, 2017). The target genes of IP were finally determined by the peaks, and the binding motifs of IP protein were called by the HOMER software (Heinz *et al*, 2010).

Chromatin immunoprecipitation (chip) sequencing

Bone marrow stromal cells were cross-linked with 1% formaldehyde for 10 min at room temperature, and nuclei were extracted, lysed, and sheared on ice. Chromatin was diluted with ChIP buffer, cleared, and incubated with 5 μg YBX1 antibody (Cell Signaling Technology, 9744S) overnight at 4°C. The antibody/chromatin complex was immunoprecipitated with protein G beads. Then, the antibody/chromatin complex was extensively washed, eluted, and de-crosslinked. After purification, ChIP DNA was used to prepare ChIP-sequencing libraries with SimpleChIP® ChIP-seq DNA Library Prep Kit for Illumina® and subjected to sequencing on an Illumina

NovaSeq6000 platform under the help of Seqhealth Technology Co., LTD (Wuhan, China). We performed the analysis of the ChIP-seq experiments as described previously (Luo *et al*, 2022). Briefly, raw sequencing data were filtered through Trimmomatic (version 0.36), and the clean reads were applied for the analysis of protein binding site. We mapped the clean reads the mouse genome (GRCm38.P6) using the STAR software (version 2.5.3a) and analyzed reads distribution using the RSeQC (version 2.6). The MACS2 software (Version 2.1.1) was used for peak calling, and the bedtools (Version 2.25.0) was used for peak annotation and peak distribution analysis. We identified the differentially binding peaks by a python script, using Fisher's test. A *P*-value < 0.05 was considered to be statistically significant enrichment.

Cycloheximide treatment

For cycloheximide treatment, cells were grown under normal conditions to approximately 80% confluence in biological replicate 10-cm plates, followed by 10-, 30-, 60-, and 120-min treatment with 50 μg/ml cycloheximide. Cells were washed three times with cold 1× PBS. Cell extracts were syringe-lysed and sonicated. Protein concentration was determined with BCA assays for subsequent western blot analysis.

Co-immunoprecipitation and Western blot analysis

For co-immunoprecipitation, BMSCs were treated with sciadopitysin or transfected with a series of HA-tagged deletion mutated YBX1 plasmid and His-tagged FBXO33 plasmid for 48 h. Total protein was extracted with Pierce IP buffer containing protease inhibitor cocktail (Selleck). Next, equal amount of protein supernatant (800 μg) was incubated with YBX1 antibody His antibody or IgG antibody overnight at 4°C. After incubating, 30 μl Protein A/G Magnetic Beads (MCE) was added to the supernatant and incubated for 2 h at 4°C. After washing for four times with IP buffer, Magnetic Beads were boiled with 2× SDS loading buffer followed by Western blotting using anti-YBX1, anti-FBXO33, anti-His, and anti-HA antibodies.

Western blot was performed as previously described. The antibodies used for Western blot are as follows: YBX1 (D299) (Cell Signaling Technology, 4202S, 1:1,000), GAPDH (Origene, TA802519, 1:5,000), PCNA (BOSTER Biological Technology, BM0104, 1:5,000), PPARGγ (81B8) (Cell Signaling Technology, 2443S, 1:1,000), P16 (Sigma-Aldrich, SAB5300498, 1:1,000), Fibronectin (Proteintech, 15613-1-AP, 1:500), SIRT2 (Abcam, ab211033, 1:1,000), FBXO33 (Novus Biologicals, NBP1-91890, 1:1,000), Neuropilin-2 (Cell Signaling Technology, 3366S, 1:1,000), RUNX2 (Abcam, ab23981, 1:1,000), SP7 (Abcam, ab22552, 1:1,000), SPP1 (Santa Cruz, sc-21742, 1:200), HA-Tag (C29F4) (Cell Signaling Technology, 3724S, 1:1,000), His-Tag (D3I1O) (Cell Signaling Technology, 12698S, 1:1,000), Ubiquitin (P4D1) (Cell Signaling Technology, 3936S, 1:1,000).

LC–MS/MS analysis

The tryptic peptides were dissolved in 0.1% formic acid (solvent A), and then loaded onto Zeba Spin columns (Pierce) in a gradient from 6% to 23% solvent B (0.1% formic acid and 98% acetonitrile). The peptides were subjected to NSI source followed by tandem mass

spectrometry (MS/MS) in Q ExactiveTM Plus (Thermo) coupled online to the UPLC. The m/z scan range was 350–1,800 for full scan, and the electrospray voltage was 2.0 kV. Peptides were then selected for MS/MS using NCE setting as 28, and the fragments were detected in the Orbitrap at a resolution of 17,500. The LC–MS/MS data were processed using Proteome Discoverer 1.3.

Molecular docking

Molecular docking was conducted as previously described (Xiao et al, 2020). Briefly, the structure of mouse YBX1 was modeled on the basis of structure of human YBX1 (PDB code:1H95) using the MODELER software for their high homology as previously described (Xiao et al, 2020). We performed virtual screening between the natural small compounds library (Target Mol, US, Boston) and YBX1 through Autodock Vina and Dock 6.7.We used the autodock tools (ADT) to set the virtual screening parameters. A small number of top-ranked compouds were purchased from Target Molecule Corp and used as candidates for further study.

Microcomputed tomography (µCT) analysis

The femurs were fixed in 4% paraformaldehyde for 24 h, then scanned and analyzed by high-resolution µCT (VIVACT 80; SCANCO Medical AG, Switzerland). Scanner was set at a current of 145 µA and a voltage of 55 kV with a resolution of 15 µm per pixel. The image reconstruction software (NRecon, version 1.6, Bioz), data analysis software (CT Analyzer, version 1.9, Bruker microCT), and 3-dimensional model visualization software (µCT Volume, version 2.0, Bruker microCT) were used to analyze the BV/TV, Tb. Th, Tb. N, and Tb. Sp of the distal femoral metaphyseal trabecular bone. The region of interest was defined as 5% of femoral length below the growth plate.

Study population

Human BMSCs cDNA were obtained by our previous study (Li et al, 2018). Human bone marrow samples were obtained from patients undergoing knee joint replacement because of osteoarthritis, undergoing hip joint replacement because of femoral neck, and/or femoral head fractures or undergoing open reduction internal fixation because of tibia or femur shaft fractures. Human bone marrow aspiration and collection were conducted by the Orthopedic Surgery Department at Xiangya Hospital of Central South University. A total of 60 patients (30 male and 30 female) were selected on the basis of the inclusion and exclusion criteria. All subjects were screened using a detailed questionnaire, disease history, and physical examination. Subjects were excluded from the study if they had conditions affecting bone metabolism or previous pathological fractures within 1 year or had received treatment with glucocorticoids, estrogens, thyroid hormone, parathyroid hormone, fluoride, bisphosphonate, calcitonin, thiazide diuretics, barbiturates, and antiseizure medication. The human studies were approved by the Ethics Committee of Xiangya Hospital of Central South University (Approval number: 2019030350). It was conducted in accordance with the principles of the Second Revision of the Declaration of Helsinki, and written informed consent was signed by every participant.

Statistics

The data are expressed as mean ± SEM. These data are normally distributed; two-tailed Student's t test is used to compare between two groups. For analysis of the statistical significance of differences between more than two groups, we performed one-way analysis of variance (ANOVA) tests with Tukey's multiple comparison tests to assess statistical significance with a 95% confidence interval. The statistics is applied by SPSS 20.0. Statistical differences were supposed to be significant when $P < 0.05$. No randomization or blinding was used, and no animals were excluded from analysis. Sample sizes were selected on the basis of previous experiments.

Data availability

All the data that support the findings of this study are available from the corresponding author upon reasonable request. The accession number for RNA sequencing data reported in this paper were list below:

BMSCs isolated from 2-month-old and 24-month-old mice: SRA: PRJNA917197 (https://www.ncbi.nlm.nih.gov/sra/PRJNA917197) and SRA: PRJNA925837 (https://www.ncbi.nlm.nih.gov/sra/PRJNA925837).
BMSCs isolated from $Ybx1^{Prx1-CKO}$ mice and $Ybx1^{flox/flox}$ mice: SRA: PRJNA917816 (https://www.ncbi.nlm.nih.gov/sra/PRJNA917816) and SRA: PRJNA908724 (https://www.ncbi.nlm.nih.gov/sra/PRJNA908724).
BMSCs transfected with shControl and shYbx1: SRA: PRJNA917816 (https://www.ncbi.nlm.nih.gov/sra/PRJNA917816).
The accession number for YBX1-CHIP data reported in this paper is: PRJNA861070 (https://www.ncbi.nlm.nih.gov/sra/PRJNA861070).
The accession number for YBX1-CLIP data reported in this paper is: PRJNA860283 (https://www.ncbi.nlm.nih.gov/sra/PRJNA860283).
The accession number for CO-IP data reported in this paper is: PXD039386.

Expanded View for this article is available online.

Author contributions

Ye Xiao: Data curation; funding acquisition; project administration.
Guang-Ping Cai: Data curation; writing – original draft. **Xu Feng:** Data curation. **Yu-Jue Li:** Data curation. **Wan-Hui Guo:** Data curation. **Qi Guo:** Validation. **Yan Huang:** Funding acquisition. **Tian Su:** Funding acquisition. **Chang-Jun Li:** Validation. **Xiang-Hang Luo:** Funding acquisition; project administration. **Yong-Jun Zheng:** Supervision; project administration. **Mi Yang:** Supervision; funding acquisition; investigation; project administration; writing – review and editing.

Disclosure and competing interests statement

The authors declare that they have no conflict of interest.

References

Allemand E, Hastings ML, Murray MV, Myers MP, Krainer AR (2007) Alternative splicing regulation by interaction of phosphatase PP2Cgamma with nucleic acid-binding protein YB-1. *Nat Struct Mol Biol* 14: 630–638

Aprile M, Cataldi S, Ambrosio MR, D'Esposito V, Lim K, Dietrich A, Bluher M, Savage DB, Formisano P, Ciccodicola A *et al* (2018) PPARgammaDelta5, a naturally occurring dominant-negative splice isoform, impairs PPARgamma function and adipocyte differentiation. *Cell Rep* 25: e1576

Baralle FE, Giudice J (2017) Alternative splicing as a regulator of development and tissue identity. *Nat Rev Mol Cell Biol* 18: 437–451

Bhadra M, Howell P, Dutta S, Heintz C, Mair WB (2020) Alternative splicing in aging and longevity. *Hum Genet* 139: 357–369

Bowler E, Oltean S (2019) Alternative splicing in angiogenesis. *Int J Mol Sci* 20: 2067

Chen Q, Shou P, Zheng C, Jiang M, Cao G, Yang Q, Cao J, Xie N, Velletri T, Zhang X *et al* (2016) Fate decision of mesenchymal stem cells: adipocytes or osteoblasts? *Cell Death Differ* 23: 1128–1139

Choi EM, Suh KS, Rhee SY, Kim YS (2014) Sciadopitysin alleviates methylglyoxal-mediated glycation in osteoblastic MC3T3-E1 cells by enhancing glyoxalase system and mitochondrial biogenesis. *Free Radic Res* 48: 729–739

Deschenes M, Chabot B (2017) The emerging role of alternative splicing in senescence and aging. *Aging Cell* 16: 918–933

Dutertre M, Sanchez G, De Cian MC, Barbier J, Dardenne E, Gratadou L, Dujardin G, Le Jossic-Corcos C, Corcos L, Auboeuf D (2010) Cotranscriptional exon skipping in the genotoxic stress response. *Nat Struct Mol Biol* 17: 1358–1366

Eliseeva IA, Kim ER, Guryanov SG, Ovchinnikov LP, Lyabin DN (2011) Y-box-binding protein 1 (YB-1) and its functions. *Biochemistry (Mosc)* 76: 1402–1433

Evans MK, Matsui Y, Xu B, Willis C, Loome J, Milburn L, Fan Y, Pagala V, Peng JC (2020) Ybx1 fine-tunes PRC2 activities to control embryonic brain development. *Nat Commun* 11: 4060

Fan X, Tang L (2013) Aberrant and alternative splicing in skeletal system disease. *Gene* 528: 21–26

Guilak F, Cohen DM, Estes BT, Gimble JM, Liedtke W, Chen CS (2009) Control of stem cell fate by physical interactions with the extracellular matrix. *Cell Stem Cell* 5: 17–26

Guo C, Xue Y, Yang G, Yin S, Shi W, Cheng Y, Yan X, Fan S, Zhang H, Zeng F (2016) Nanog RNA-binding proteins YBX1 and ILF3 affect pluripotency of embryonic stem cells. *Cell Biol Int* 40: 847–860

Harries LW, Hernandez D, Henley W, Wood AR, Holly AC, Bradley-Smith RM, Yaghootkar H, Dutta A, Murray A, Frayling TM *et al* (2011) Human aging is characterized by focused changes in gene expression and deregulation of alternative splicing. *Aging Cell* 10: 868–878

Heinz S, Benner C, Spann N, Bertolino E, Lin YC, Laslo P, Cheng JX, Murre C, Singh H, Glass CK (2010) Simple combinations of lineage-determining transcription factors prime cis-regulatory elements required for macrophage and B cell identities. *Mol Cell* 38: 576–589

Jayavelu AK, Schnoder TM, Perner F, Herzog C, Meiler A, Krishnamoorthy G, Huber N, Mohr J, Edelmann-Stephan B, Austin R *et al* (2020) Splicing factor YBX1 mediates persistence of JAK2-mutated neoplasms. *Nature* 588: 157–163

Kim D, Langmead B, Salzberg SL (2015) HISAT: a fast spliced aligner with low memory requirements. *Nat Methods* 12: 357–360

Kohno K, Izumi H, Uchiumi T, Ashizuka M, Kuwano M (2003) The pleiotropic functions of the Y-box-binding protein, YB-1. *Bioessays* 25: 691–698

Kotake Y, Ozawa Y, Harada M, Kitagawa K, Niida H, Morita Y, Tanaka K, Suda T, Kitagawa M (2013) YB1 binds to and represses the p16 tumor suppressor gene. *Genes Cells* 18: 999–1006

Lee Y, Rio DC (2015) Mechanisms and regulation of alternative pre-mRNA splicing. *Annu Rev Biochem* 84: 291–323

Li CJ, Cheng P, Liang MK, Chen YS, Lu Q, Wang JY, Xia ZY, Zhou HD, Cao X, Xie H *et al* (2015) MicroRNA-188 regulates age-related switch between osteoblast and adipocyte differentiation. *J Clin Invest* 125: 1509–1522

Li H, Liu P, Xu S, Li Y, Dekker JD, Li B, Fan Y, Zhang Z, Hong Y, Yang G *et al* (2017) FOXP1 controls mesenchymal stem cell commitment and senescence during skeletal aging. *J Clin Invest* 127: 1241–1253

Li CJ, Xiao Y, Yang M, Su T, Sun X, Guo Q, Huang Y, Luo XH (2018) Long noncoding RNA Bmncr regulates mesenchymal stem cell fate during skeletal aging. *J Clin Invest* 128: 5251–5266

Luo L, Liu Y, Nizigiyimana P, Ye M, Xiao Y, Guo Q, Su T, Luo X, Huang Y, Zhou H (2022) DNA 6mA demethylase ALKBH1 orchestrates fatty acid metabolism and suppresses diet-induced hepatic steatosis. *Cell Mol Gastroenterol Hepatol* 14: 1213–1233

Lutz M, Wempe F, Bahr I, Zopf D, von Melchner H (2006) Proteasomal degradation of the multifunctional regulator YB-1 is mediated by an F-box protein induced during programmed cell death. *FEBS Lett* 580: 3921–3930

Lyabin DN, Eliseeva IA, Ovchinnikov LP (2014) YB-1 protein: functions and regulation. *Wiley Interdiscip Rev RNA* 5: 95–110

Ma S, Sun S, Geng L, Song M, Wang W, Ye Y, Ji Q, Zou Z, Wang S, He X *et al* (2020) Caloric restriction reprograms the single-cell transcriptional landscape of Rattus Norvegicus aging. *Cell* 180: 984–1001.e22

Maier B, Gluba W, Bernier B, Turner T, Mohammad K, Guise T, Sutherland A, Thorner M, Scrable H (2004) Modulation of mammalian life span by the short isoform of p53. *Genes Dev* 18: 306–319

Makita N, Suzuki M, Asami S, Takahata R, Kohzaki D, Kobayashi S, Hakamazuka T, Hozumi N (2008) Two of four alternatively spliced isoforms of RUNX2 control osteocalcin gene expression in human osteoblast cells. *Gene* 413: 8–17

Marchesini M, Ogoti Y, Fiorini E, Aktas Samur A, Nezi L, D'Anca M, Storti P, Samur MK, Ganan-Gomez I, Fulciniti MT *et al* (2017) ILF2 is a regulator of RNA splicing and DNA damage response in 1q21-amplified multiple myeloma. *Cancer Cell* 32: 88–100.e6

Mazin P, Xiong J, Liu X, Yan Z, Zhang X, Li M, He L, Somel M, Yuan Y, Phoebe Chen YP *et al* (2013) Widespread splicing changes in human brain development and aging. *Mol Syst Biol* 9: 633

Milona MA, Gough JE, Edgar AJ (2003) Expression of alternatively spliced isoforms of human Sp7 in osteoblast-like cells. *BMC Genomics* 4: 43

Ott SM (2008) Histomorphometric measurements of bone turnover, mineralization, and volume. *Clin J Am Soc Nephrol* 3: S151–S156

Pan Q, Shai O, Lee LJ, Frey BJ, Blencowe BJ (2008) Deep surveying of alternative splicing complexity in the human transcriptome by high-throughput sequencing. *Nat Genet* 40: 1413–1415

Park JW, Fu S, Huang B, Xu RH (2020) Alternative splicing in mesenchymal stem cell differentiation. *Stem Cells* 38: 1229–1240

Peffers MJ, Goljanek-Whysall K, Collins J, Fang Y, Rushton M, Loughlin J, Proctor C, Clegg PD (2016) Decoding the regulatory landscape of ageing in musculoskeletal engineered tissues using genome-wide DNA methylation and RNASeq. *PLoS One* 11: e0160517

Pittenger MF, Mackay AM, Beck SC, Jaiswal RK, Douglas R, Mosca JD, Moorman MA, Simonetti DW, Craig S, Marshak DR (1999) Multilineage potential of adult human mesenchymal stem cells. *Science* 284: 143–147

Sekiya I, Larson BL, Vuoristo JT, Cui JG, Prockop DJ (2004) Adipogenic differentiation of human adult stem cells from bone marrow stroma (MSCs). *J Bone Miner Res* 19: 256–264

Shah A, Lindquist JA, Rosendahl L, Schmitz I, Mertens PR (2021) Novel insights into YB-1 signaling and cell death decisions. *Cancers (Basel)* 13: 3306

Shi Y (2017) Mechanistic insights into precursor messenger RNA splicing by the spliceosome. *Nat Rev Mol Cell Biol* 18: 655–670

Skabkin MA, Liabin DN, Ovchinnikov LP (2006). [Nonspecific and specific interaction of Y-box binding protein 1 (YB-1) with mRNA and posttranscriptional regulation of protein synthesis in animal cells]. *Mol Biol (Mosk)* 40: 620–633

Southworth LK, Owen AB, Kim SK (2009) Aging mice show a decreasing correlation of gene expression within genetic modules. *PLoS Genet* 5: e1000776

Suh KS, Lee YS, Kim YS, Choi EM (2013) Sciadopitysin protects osteoblast function via its antioxidant activity in MC3T3-E1 cells. *Food Chem Toxicol* 58: 220–227

Urbanski LM, Leclair N, Anczukow O (2018) Alternative-splicing defects in cancer: splicing regulators and their downstream targets, guiding the way to novel cancer therapeutics. *Wiley Interdiscip Rev RNA* 9: e1476

Uren PJ, Bahrami-Samani E, Burns SC, Qiao M, Karginov FV, Hodges E, Hannon GJ, Sanford JR, Penalva LO, Smith AD (2012) Site identification in high-throughput RNA-protein interaction data. *Bioinformatics* 28: 3013–3020

Wang E, Lu SX, Pastore A, Chen X, Imig J, Chun-Wei Lee S, Hockemeyer K, Ghebrechristos YE, Yoshimi A, Inoue D *et al* (2019) Targeting an RNA-binding protein network in acute myeloid leukemia. *Cancer Cell* 35: 369–384.e7

Wei WJ, Mu SR, Heiner M, Fu X, Cao LJ, Gong XF, Bindereif A, Hui J (2012) YB-1 binds to CAUC motifs and stimulates exon inclusion by enhancing the recruitment of U2AF to weak polypyrimidine tracts. *Nucleic Acids Res* 40: 8622–8636

Xia H, Chen D, Wu Q, Wu G, Zhou Y, Zhang Y, Zhang L (2017) CELF1 preferentially binds to exon-intron boundary and regulates alternative splicing in HeLa cells. *Biochim Biophys Acta Gene Regul Mech* 1860: 911–921

Xiao YZ, Yang M, Xiao Y, Guo Q, Huang Y, Li CJ, Cai D, Luo XH (2020) Reducing hypothalamic stem cell senescence protects against aging-associated physiological decline. *Cell Metab* 31: 534–548.e5

Yang M, Li CJ, Sun X, Guo Q, Xiao Y, Su T, Tu ML, Peng H, Lu Q, Liu Q *et al* (2017) MiR-497 approximately 195 cluster regulates angiogenesis during coupling with osteogenesis by maintaining endothelial notch and HIF-1alpha activity. *Nat Commun* 8: 16003

Zhang Y, Huang YX, Wang DL, Yang B, Yan HY, Lin LH, Li Y, Chen J, Xie LM, Huang YS *et al* (2020) LncRNA DSCAM-AS1 interacts with YBX1 to promote cancer progression by forming a positive feedback loop that activates FOXA1 transcription network. *Theranostics* 10: 10823–10837

Zhou BO, Yue R, Murphy MM, Peyer JG, Morrison SJ (2014) Leptin-receptor-expressing mesenchymal stromal cells represent the main source of bone formed by adult bone marrow. *Cell Stem Cell* 15: 154–168